THESIS

NEUTRON FLUENCE IN A HOWITZER DRUM AND CONSTRUCTION OF A WATER MODERATED NEUTRON IRRADIATOR

Submitted by

Anilu S. Diaz Ruiz

Department of Environmental and Radiological Health Sciences

In partial fulfillment of the requirements

For the Degree of Master of Science

Colorado State University

Fort Collins, Colorado

Summer 2024

Master's Committee:

Advisor: Ralf Sudowe

Thomas Johnson

Gwen Fisher

ABSTRACT

NEUTRON FLUENCE IN A HOWITZER DRUM AND CONSTRUCTION OF A WATER MODERATED NEUTRON IRRADIATOR

The Department of Environmental and Radiological Health Sciences at Colorado State University is utilizing a variety of irradiators to study the effects of ionizing on materials and tissue. Two of these are neutron irradiators based on 1 Ci and 5 Ci plutonium/beryllium (PuBe) sources, respectively. Neutron activation analysis is utilized to measure the neutron fluence at various positions in a Neutron Howitzer containing the 5 Ci source and a water tank containing the 1 Ci source. By determining the neutron flux in both systems, neutron irradiation at different intensities will become available for future research at Colorado State University. Additionally, both the drum and tank will be excellent teaching tools as they demonstrate neutron moderation, neutron shielding, material activation, and fluence measuring. Manufactured by the Nuclear-Chicago Corporation, the Model NH-3 Neutron Howitzer Drum is constructed in such a fashion that the PuBe neutron source can be moved in and out of irradiation position. In the irradiation position, two samples may be exposed to neutrons from the source by placing them in one of two horizontal ports in the drum. Both drum and ports are shielded with paraffin, which allows moderation of the neutron flux to thermal energies. In the experimental study, multiple metal foils were activated in the drum by irradiating them up to the point of measurable activity. Using a High Purity Germanium (HPGe) detector, the activity of the foils is quantified. The results of the measurements were used to calculate the neutron fluence using known neutron capture cross-sections. The calculated neutron fluence was then compared to the neutron fluence determined

through a computational model of the drum using the Monte-Carlo N-Particle transport code (MCNP). Using the principles and methods practiced on the Howitzer drum, a water moderated neutron tank was constructed as a secondary neutron irradiator. The compared experimental and modeled neutron fluence spectrum in the drum were used to derive an effective model for total neutron fluence with respect to spacing from the inner end of the sample channel (x) of $y = 69759e^{-0.17x}$ and thermal neutron fluence of $y = 12035e^{-0.176x}$.

ACKNOWLEDGMENTS

I would like to give thanks to my professors and peers who have lent a helping hand whenever needed. A special thanks is given to my advisor for his help and patience, and the Workman family for lending their equipment, experience, and time to me in efforts of constructing the water moderated tank.

An even bigger acknowledgement is to be given to my furry babies for serving as my emotional support stress toys and keeping me sane through the most challenging times.

TABLE OF CONTENTS

CHAPTER 1: INTRODUCTION

1.1 **Neutrons**

In the 1930's, J. Chadwick published his findings of a new sub-atomic particle critical in the composition of matter. The discovery described a neutral charge particle slightly heavier than a proton that is contained in the nucleus [1]. Since their discovery, neutrons have been researched in depth in the past century. Today, neutrons are well understood regarding their unique characteristics and behavior in matter. Free neutrons are understood to always originate from a nucleus and are described to be born "fast". These free neutrons are categorized by their kinetic energy as a general description of their energy and expected behavior [2]. The names and energy ranges of these descriptive categories are not standardized and may vary when comparing documents. However, to describe these energy ranges in this report, Table 1 lists the categories and energy ranges used in this work. The specifics of these categories are given by Lawrence Heilbronn in the supplementary report "Neutron Properties and Definitions" are used [3].

Table 1: Neutron energy categories with corresponding energy ranges [3]. Class-terms are used to describe like-energy categories to reduce the need to remember specific energy ranges.

Class	Category	Energy Range
Thermal	Cold	0- 0.025 eV
	Thermal	0.025 eV
Slow	Epithermal	0.025 - 100's keV
	Slow	100's keV – 1 MeV
Fast	Fast	1 MeV - 20 MeV
	Relativistic	> 20 MeV

In the work summarized in this report, neutrons are referred to in the general classification terms, thermal, slow, and fast. This was done to facilitate the analysis. However, it is important to

note that these energy ranges are not standardized and describe the intensity of energy rather than discrete energy ranges.

Neutrons are described by their kinetic energy due to the dependency of their interactions in matter on it. Since neutrons are neutral in electric charge, they interact via kinetic interactions such as elastic and inelastic scattering instead of coulombic force-based interactions. Scattering is dependent on the physical interaction between the neutron and the nucleus which has sufficient mass to interfere with the particle's trajectory. However, if no interference occurs with a nucleus, the neutron remains on its path undisturbed [4]. A descriptor of the probability for a neutron interaction are cross-sections. A cross-section is defined as the probability of interaction in a medium from a neutron of a given energy per unit area. As a general principle, neutron cross-sections have an inverse proportionality to the neutron's velocity [5]. Canonically, cross-sections are described in the unit of Barns which equates to 10^{-24} cm^2 [6]. When paired with the volume of the medium (or number of nuclei target), cross-sections can be converted to units of length traveled before an interaction. Cross-sections are heavily dependent on neutron energy and can be reported for each interaction type or as a sum of all interactions (interaction types will be discussed later in section 1.1.1). In other words, sum cross-sections becomes the probability per unit length that any neutron interaction will occur in a material [4]. Another descriptor of the nucleus behavior after a neutron induced reaction is the Q-value, which refers to the mass-energy available after a reaction [6]. However, cross-sections are more intuitive to understand, describe, and to use in practical settings.

1.1.1 Neutron Interactions

As mentioned in the previous section, neutron interactions are dependent on the incident neutron's initial energy. In the lower energy ranges, neutron interactions are easily described since they follow basic physics. However, at higher energies neutrons reach a point where they may undergo a nuclear reaction or reactions that are not as obvious as with the slower neutrons. In this section, neutron interactions per class are described to provide an understanding of the scope of the thesis work done.

The simplest neutron interaction occurs when a thermal neutron is absorbed into a nucleus. The absorption of the neutron changes the mass number of the nuclide and may result in an imbalance of energy. A description of this reaction is stated in *Neutron Activation Analysis* as, "Conservation of energy includes the energy corresponding to the difference of mass during the reaction, that is the most important fraction of the available kinetic energy. If the total mass diminishes, the corresponding energy (E=mc^2) is thus released as kinetic energy of the emitted particles or as the energy of a photon of the residual nucleus". These emitted gamma rays can be as high as 9 MeV, depending on the nucleus type [4]. In terms of Q-values, a positive value describes a reaction where the residual mass-energy (Q-value given in a.m.u. or eV) may be used as kinetic energy for the nucleus or excites the nucleus into gamma decay [6]. Hence, the absorption of a thermal neutron may cause a change in the nucleus resulting in radiation decay which is referred to as neutron activation. In section 1.2 neutron activation will be discussed in further detail.

Neutrons in the slower range of energy typically interact via elastic scattering. In this type of collision, the kinetic energy of the system is conserved in a collision between the neutron and nucleus [4]. Elastic scattering is commonly thought of as the interaction of two masses where the

masses are either $M_1 < M_2$, $M_1 = M_2$, or $M_1 > M_2$. The ratio of the two masses will determine the distribution of the energy after the interaction [2]. In most absorbing mediums, elastic scattering is very probable for slow neutrons and will result in slight recoil of the nuclei and thermalization of the neutron. Slightly faster neutrons may interact via inelastic scattering which does not conserve kinetic energy in the system. This interaction results in the excitation of a nucleus as the neutron collides with it. The excited nucleus can then emit a photon to revert to its ground state. In this interaction the nucleus absorbs the neutron but then simultaneously emits another but with lower energy. The difference in energy is then emitted from the nucleus as a gamma ray. This inelastic reaction has a threshold probability of occurrence for a given medium [2]. Collisions often serve to bring slow neutrons into thermal equilibrium with the absorber medium and they are ultimately absorbed. As mentioned previously, slow neutron interaction or absorption may result in the (n, gamma) reaction which produces secondary radiation [4]. The generation of gammas may be used to measure when a neutron reaction has occurred. This will be discussed more in detail in the detection section.

Neutrons with sufficient energy to be described in units of MeV are referred to fast neutrons. Due to their high energy, interactions between the free neutron and matter exhibit a different behavior than previously discussed. Not only do neutrons that scatter have a much larger travel range in which they scatter, but they may also induce a different type of reaction. In a similar reaction to inelastic scattering, the de-excitement of the nucleus may emit a gamma of relatively large energy (in MeV) or result in neutron activation of the material [4]. In reactions at large neutron energies, the activation product may be a different radionuclide than those in thermal neutron activation. In section 1.3, activation from fast neutrons is discussed further.

1.1.2 Neutron Shielding and Moderation

Elastic collisions define a physical interaction between matter in a system in which there is no loss of kinetic energy. In these interactions, the quantity of energy transferred to a target through the collision is dependent on the target mass, and so, most of the kinetic energy in the mass incident is transferred to the target if they are equal in mass. This concept is the basis of moderating materials, which are used to slow down neutrons. Thus, materials containing high quantities of hydrogen make the most effective moderators as neutrons may transfer up to 63% of their kinetic energy to hydrogen since they are similar in mass [2]. Materials commonly used for neutron moderation and shielding include water, concrete, paraffin, and plastics [4].

Calculating shielding thicknesses required for neutrons can quickly become complicated due to the neutrons scattering behavior and their potential to induce secondary radiation. However, for the purposes of quick neutron moderation and shielding assessments, diffusion lengths for fast and slow neutrons are used. Their use in calculations is an approximation and simplifies the repeated energy loss per scatter to energy loss in a length of a material. Diffusion lengths are an average straight path length which a neutron may travel through the medium until it becomes thermal and absorbed. However, it is important to emphasize that these values are only an estimate and should not replace measurable quantities is possible. In Table 2, common diffusion lengths for frequently used shielding material for fast and thermal neutrons are listed. In combination to the diffusion lengths, Equation 1 is used to calculate the moderation of a neutron beam through the diffusion length of a material [2].

Table 2. Diffusion lengths for fast and thermal neutrons in common moderating materials.

Material	Fast Diffusion Length (cm)	Thermal Diffusion Length (cm)
Light Water	5.75	2.88
Heavy Water	11	171
Graphite	17.3	24
Beryllium	9.9	50

$$n = n_o e^{-(\frac{T}{L})} \quad \text{(Equation 1)}$$

Where N_o = initial intensity of the neutron beam

T = thickness of the shielding material (cm)

L = diffusion length (cm)

1.2 **Neutron Activation**

The principle of neutron activation may be used to carry out indirect measurements of unbound neutrons in an environment or laboratory sample. Neutron activation analysis is a form of non-destructive analysis of a sample through inducing neutron activation in the material [4]. Materials commonly used in NAA are known as activation detectors and consist of thin pieces of materials with high neutron cross-sections (thermal or resonance), usually in the form of a very thin foil or wire. The thinness of the activation detectors is a key characteristic of these materials since neutron attenuation or moderation in the material would increase the uncertainty in the subsequent neutron fluence calculations. The use of NAA is a helpful technique which may be utilized to determine magnitudes of neutrons and can be calculated as a flux or fluence. However, it is imperative to remember that neutron activation is an integral activation of the

material but will need to be corrected for the eventual decay of the activation products. Therefore, if the neutron fluence investigated continuously changes (such as a moving source, or quantity of source changes through time) then the activation products measured are an integral of all the neutrons which induced a reaction in a total time. Likewise, the measured activation products of a given isotope correspond to a certain neutron energy (sometimes a small range of energies of similar magnitudes) [5]. A useful calculation which is done in NAA is the saturation activity. This calculation is shown in Equation 2, and it is the final activity of a sample if irradiated for an infinite time. Thus, the saturated activity is the resultant activity of activation and decay in equilibrium [4]. As discussed previously, all neutron activation calculations are neutron energy dependent. Then, when Equation 3 is decay corrected, the resultant activity of the sample after time t is shown in Equation 3. Generally, the equation describes the proportionality of the sample's activity to irradiation time, till it reaches its saturated activity. The time of exposure is an imperative factor which will impact the activity of sample, and so, affecting the precision of measurements. Hench, as a general principle, it is advised that shot irradiation times for short-lived products and vice versa for long-lived products in neutron activation [5].

$$Saturated\ Activity = \phi_i \sigma_i N_T \qquad \text{(Equation 2)}$$

Where σ_i = neutron cross-section for energy i in material (barns),

ϕ_i = i energy neutron fluence (n/cm^{2}s),

N_T = number of target atoms.

$$Activity = SA(1 - e^{-\lambda t_{irr}}) \quad \text{(Equation 3)}$$

Where SA = Saturated Activity (dps),

λ = decay constant (1/s)

t_{irr} = irradiation time (s).

In the previous sections, thermal interactions resulting in neutron absorption have been briefly described. The potential synthesis of a radioisotope through a neutron interaction may be referred to as neutron activation. Notably, neutron activation is not restricted to only thermal neutrons but may also occur with slow and fast neutrons [2]. In neutron activation analysis (NAA), activation from thermal/slow neutrons may be distinguished from activation of faster neutrons via the cadmium ratio (CR). The CR method uses cadmium's high cross-section for neutrons below 0.4 eV to calculate the difference between activation of a foil from epithermal and slow neutrons [6]. These neutrons with higher energy than thermal neutrons that also may induce neutron activation are referred to as resonance neutrons. The calculation for the CR is shown in Equation 4 [4]. In elemental trace analysis, methods such as NAA provide desirable high sensitivity. As described in *Neutron Activation Analysis*, NAA has a sensitivity of 0.001 ppm with good specificity and accuracy, while other trace analysis methods such as mass spectrometry do not perform to this degree of sensitivity or accuracy. However, it is important to remember that the sensitivity of NAA increases with neutron fluence intensity such as the fluences found in research reactors [6]. The use of non-destructive NAA provides the ability to differentiate elemental compositions of samples to a standard. The analysis also provides variability in sample matrices along with reducing the need of a large sample mass [6].

$$CR = \frac{Actavation_{bare\ foil}}{Activation_{Cd\ covered\ foil}} \quad \text{(Equation 4)}$$

Table 3 lists all the neutron thermal and integral cross-sections for the elements used in this work. As previously mentioned, the cadmium ratio allows the comparison of activation from thermal and resonance neutrons. Therefore, resonance cross-sections are used to calculate the resonance energy fluence experienced by the foil. Resonance cross-sections are the probability of activation from higher energy neutrons where the range of resonance energies for the cross-sections given are from 0.5 eV to infinity [7]. The high energy bound for resonance cross-sections are defined at infinity since the energy bound will differ for each material. Regardless of the defined energy bounds given for resonance cross-sections, previous activation works have narrowed the upper resonance energy bounds for neutron in Au and In to be 5 keV and 2.43 eV respectively [8, 9]. All thermal and resonance neutron cross-sections and natural abundances were sourced from the document *Thermal Neutron Capture Cross-Sections Resonance Integrals And G-Factors* by Mughabghab, which compiled cross-sections from various works and compared their results [10].

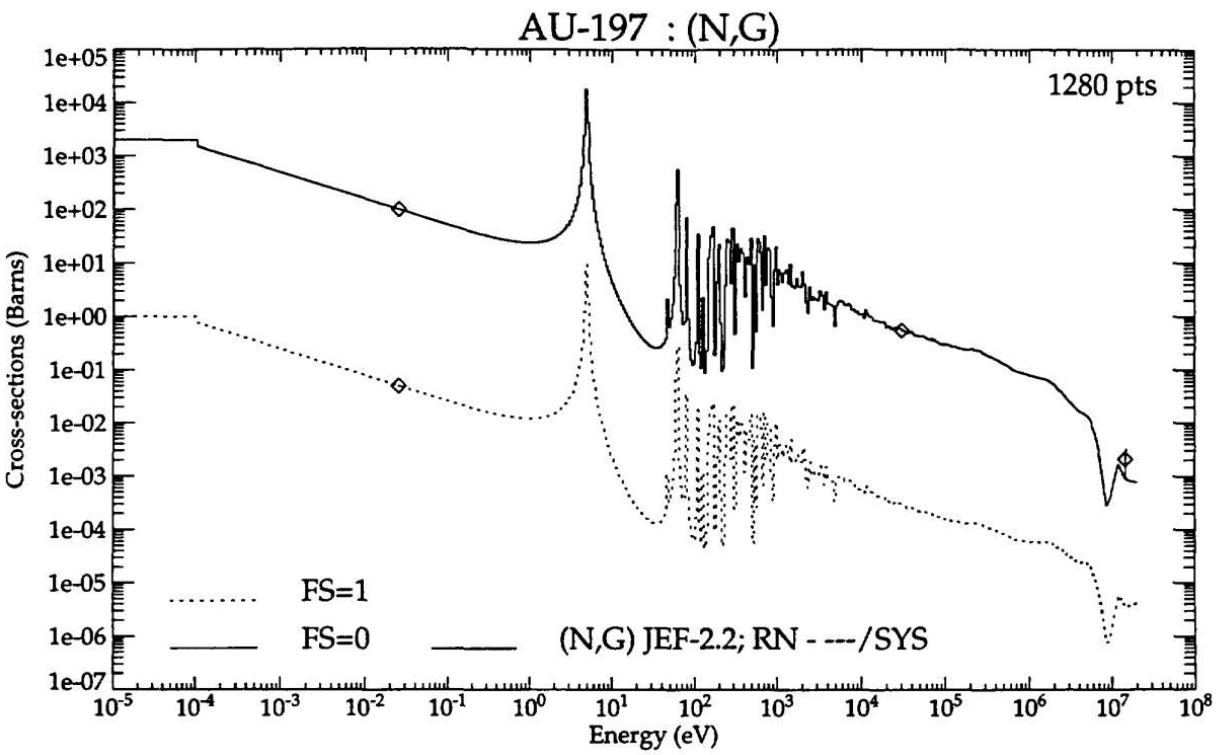

Figure 1: Example of neutron activation cross-sections plotted with respect to neutron energy. As seen, a very large cross-section is shown at very low energies which is referred to as the thermal cross-section. Past thermal energies, the value decreases as the energy increases. However, at mid-energies there are spikes in the cross-sections. These peaks are integrated to produce the resonance cross-section [11].

Table 3: List of characteristics for activation foils used. The thermal neutron cross-sections, resonance cross-sections and details of activation products induced by these neutrons are listed below.

Element	Thermal Cross Section (b)	Resonance Cross Section (b)	Half-Life	Activation Product	Gamma (MeV)	Branching Ratio
Gold	98.65±0.09	1550±28	2.6941±0.0004 day	Au-198	0.411	1
Indium	202±2	3300±100	54.29 ±0.17 min	In-116m	1.294	0.848±0.012
					1.097	0.585±0.008
					0.417	0.272±0.004
					2.112	0.151±0.0022
					0.819	0.121±0.0014

1.3 Threshold Reactions

There are many types of fast neutron interactions which may induce measurable interactions. These reactions are generated through the absorption of a fast free neutron into a nucleus causing it to become unstable. As a result, secondary radiation may be emitted as the nucleus decays to regain stability [3]. In terms of the Q-value, a negative value describes an endergonic reaction, requiring a threshold neutron energy to induce a nuclear reaction [6]. Some common threshold reactions are (n, alpha), (n, p), (n, n') where the product is radioactive. Reactions that result in a charge change such as (n. alpha) are the result of incident neutrons with energies large enough to overcome the coulombic barrier. In addition, the neutron energy must be sufficiently high to provide kinetic energy to the particles emitted by the nucleus [6]. Due to all these energetic parameters, the reactions are referred to as "threshold activations". If the primary or secondary radiation from the product is easily measurable, such as a gamma, then the occurrence of the fast neutron interaction may be measured and quantified [5]. In terms of cross-sections, an interaction for a fast neutron is virtually zero for most materials, however there are some elements that will have a non-zero cross-section for fast neutrons. That is, past a threshold neutron energy the cross-section increases to some non-zero amount. These materials are therefore optimal to measure activation at these threshold energies. In this work, a broad-spectrum foils kit manufactured by Shieldwerx containing an array of metal foils was used to supply the foils used for NAA. Listed below is the foil used for threshold NAA in this document. All values detailing the threshold activations were sourced from the Evaluated Nuclear Data Files (ENDF) and are listed in Table 4 along with activation details [12].

Table 4: List of characteristics for threshold activation in In foils.

Element	Half-Life	Activation Product	Measurable Gamma (MeV)	Branching Ratio
Indium	4.486±0.004 hr	In-115m	0.336	0.459±0.001

1.4 **Neutron Howitzer**

Neutron howitzer are tools designed to demonstrate neutron interaction and neutron activation through the simple design of a drum filled with a moderator and a neutron source [13]. The principle behind the design of a neutron howitzer drum is to produce a large intensity of slow-energy neutron fluence from a neutron source via the geometrical design of the drum and its moderating material [14]. Materials such as water, paraffin, or wood may be used as moderators. However, the simplest of these materials to use is paraffin since any volume may be filled when the material is melted and becomes hard once cooled. The use of paraffin also reduces the drum's necessity to be watertight long-term, unlike when water is used [15].

A Nuclear Chicago Instruments Neutron Howitzer NH-3 was used in this thesis. The key dimensions of the drum are listed in Table 5. The model NH-3 neutron howitzer is primarily an aluminum drum filled with paraffin as the neutron moderator. At the center of the drum, two sample channels contain a drawer in which samples may be placed. Plastic cylindrical spacers are provided with the drawer and are used to moderate the air in the sample channel around the sample. The spacers are an additional method to estimate the distance of the sample from the front of the sample channel, as four 4 cm and four 2 cm spacers can be used in combination in the drawer.

Table 5: Dimensions of Neutron Howitzer drum used in MCNP modeling.

Feature	Thickness (cm)
Drum Height	88.9
Drum Radius	28.575
Drum Al Thickness	0.3
Source Channel Length	55.88
Source Channel Thickness	0.1
Source Channel Radius	1.666875
Sample Port Length	26.67
Sample Port Thickness	0.1
Sample Port Inner-Radius	2.69875
Source Length	18.0975
Source Radius	1.42875
Source Cladding Thickness	0.1

At the center top of the drum, a Plexiglas rod is used to lift the source out of its shielded position to an exposed position. When exposed, the source is directly centered in between the sample channels. With the source rod lifted, the samples are exposed to the full neutron energy spectrum, however the moderating material greatly increases the magnitude of thermal neutrons along the sample channel compared to an air-filled drum [13]. Figures 2 and 3 show a picture of the Neutron Howitzer used for NAA and the internal components of the sample channels.

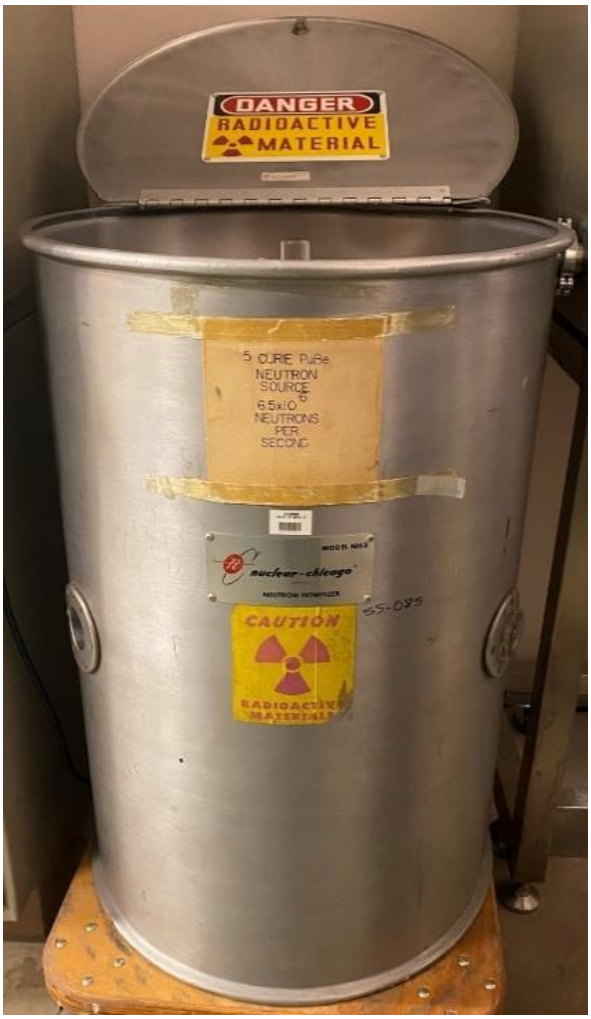

Figure 2: Neutron Howitzer NH-3 drum containing 5 Cu PuBe source.

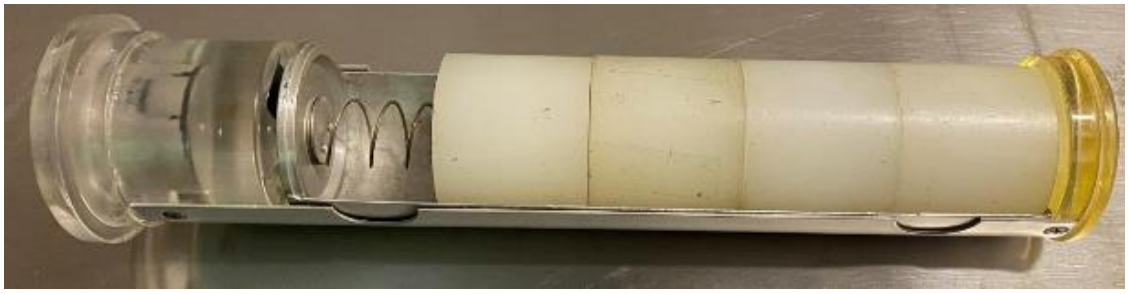

Figure 3: Sample channel of Neutron Howitzer NH-3 drum. The right end of the drawer faces the source and the left end faces the outer surface of drum. Four plastic spaces are contained inside the sample channel.

1.5 **(Alpha, n) Sources**

The decay of an isotope through the emission of a neutron is not typically observed because the energy required to overcome the neutron binding energy is too large for most naturally occurring reactions. Thus, neutron sources are either based on spontaneous fission, such as Cf-252, or on induced neutron emission through a nuclear reaction [4].

Manufactured neutron sources are commonly composed of a mixture of elements which induce a nuclear reaction, emitting neutrons of a discrete energy or more commonly, a wide energy range. After the discovery of neutron induced radioactivity in 1934, Enrico Fermi led multiple studies exploring the topic with various manufactured neutron sources [16]. A common reaction used to produce neutrons is the (alpha, n) reaction. For alpha induced neutron sources, the alpha emitter typically consists of Ra, Po, Pu, or Am powder that is uniformly mixed with beryllium powder [2]. Sources are usually contained in a small canister and are sealed to prevent any material form of leaking in normal conditions. Alpha induced sources produce a neutron energy spectrum based on the kinetic energy of the initial alpha particle and the mass-energy available after the reaction. Since sources are uniformly mixed, a small fraction of self-absorption and moderation occurs for the low energy neutrons produced in the center of the volume. Hence, measured neutron energy spectrums are mostly composed of slow to fast energy neutrons. Table 6 lists the properties of some common beryllium (alpha, n) sources.

Table 6: Traits of common (alpha, n) sources used in laboratories [2,4].

Source	Half-Life	Average Alpha Energy (MeV)	Average Neutron Energy (MeV)	Average Neutron Yield ((n/s)Ci)
^{239}PuBe	24000 yrs	5.14	4	10^6
^{210}PoBe	138 d	5.3	4	$3x10^6$
^{226}RaBe	1600 yrs	multiple	5	$1.7x10^7$

1.5.1 PuBe Sources

Two neutron PuBe sources were used for neutron activation in this work. One source is reported to have an activity of 5 Ci (1E7 n/s), or as stated on the safety plan, have a fluence of 1E5 n/s cm^2 at the surface of the casing [17]. The source is described to be 1 inch in diameter and 1inch in length. The second PuBe source has an activity of 1 Ci (2E6 n/s). Information regarding the sources' calibration date or manufacturers was unavailable. Having limited information regarding a neutron source is unfortunately common, as documentation for such old materials may not have been provided by sellers or has been misplaced through the years. However, correcting for decay is not an issue for experimental purposes when working with PuBe source due to the very long half-life of the Pu-129.

1.6 **HPGe Gamma Detection and Measurement**

High-purity germanium (HPGe) detectors are used to measure the radioactivity of a sample emitting gamma radiation. The detector is classified as a p-type semiconductor germanium crystal. A key characteristic of HPGe detectors which differentiates them further from common gamma spectrometry instruments is the need to keep the crystal at a cold temperature (~77 K), typically done through bringing the crystal in contact with a supply of liquid nitrogen. When determining which instrument to use for gamma spectrometry, resolution is often a deciding factor, and so HPGe detectors are more popularly used over other detectors such as a NaI(Tl) detectors. Hence, if quantification of energy deposit is more precise then the variance reduces which in turn also reduces the area under the photopeak. A method to quantify resolution in spectrometry is through the Full Width Half Maximum (FWHM). High resolution is

desired for spectrometry as it helps in distinguishing peaks from each those with small counts with background. Hence, a spectrum with a small FWHM has better resolution than one with a larger FWHM. As stated in Gilmore, the FWHM at 661.67 keV (Cs-137) is 0.794 and 25 channels for an HPGe and NaI(Tl) detectors, respectively [18]. HPGe detectors therefore have a better resolution than NaI(Tl) detectors. However, using an HPGe comes with its own challenges such as its need to stay in cryostasis. Regardless of the additional challenges, the spectrometry done in this report was performed with two HPGe detectors with a relative efficiency of 35%. These detectors are shown in Figure 4 as pictures of the lead shielding and detector setup.

Figure 4: HPGe detectors used in this report, named Joliot and Curie.

Gamma spectroscopy is the measurement and recording of radiation quanta from a sample into a spectrum. As discussed above, detectors such as HPGe detectors may be used to record these spectra of activity and energy. To correctly measure a spectrum from a sample, the detector and accompanying electronics must be set up properly to assure the detector and electronics are not damaged and to reduce electrical noise which increases background measurements. Once the detector is set up and ready to measure, the system must be calibrated for energy. This is typically done by measuring a variety of sources with different photo peak energies to form a linear relationship between event energy and channel number that can be stored in the Multi-Channel Analyzer (MCA). After a gamma spectrum has been measured and recorded, the process of analyzing the peaks is referred to as spectrometry. In gamma spectrometry, the region of interest (ROI) is analyzed in a spectrum. For a simple gamma source, the ROIs are photopeaks and their corresponding Compton continuum. An additional factor that is measured apart from the spectrum is the dead time of the measuring process. Dead time is the time when the electronics are busy processing data and are therefore not able to measure events occurring, and live time is when the detector is available to count. Due to dead time, live time will often be longer than real time. Thus, the dead time can be used to understand how active a sample is in comparison to background or other samples. Dead time is also used to correct the measuring time of the spectrum.

Gamma spectroscopy and spectrometry are common analysis methods used in NAA. Through the measurement and quantification of gammas observed by a detector (counts), a calculation of activity may be performed to propose an initial activity for a sample. There are many factors that must be taken into consideration when conducting gamma spectrometry, such as geometry, reproducibility, efficiency and sample decay. An additional factor that cannot be

neglected for NAA is the possibility of pair production for gamma emitters above 1.02 MeV (NAA). Thus, some spectra may show peaks for the positron annihilation, escape peaks, or sum peaks for the expected peaks from each activated sample. This thesis work uses the software Genie 2000 version 3.4 by Canberra to facilitate spectrometry analysis such as determining peak detection, peak area counts, background correction, and efficiency correction.

To report any form of decay rate from the measured spectrum, counts measured must be corrected using the detectors efficiency. The absolute total efficiency is used to convert the number of counts measured for a photopeak to the number of gamma decays originating from the source. The conversion for activity from counts is shown in Equation 5.

$$dpm = \frac{cpm}{\varepsilon} \qquad \text{(Equation 5)}$$

Where dpm = counts per minute, energy dependent,

dpm = counts per minute, energy dependent,

ε = Instrument efficiency, energy dependent.

1.7 MCNP

In the world of radiation transfer and particle tracking, a tool used by professionals in various fields is Monte-Carlo N-Particle transport code (MCNP). As stated in the MCNP 3.6 user manual, “The MCNP code is a general-purpose, continuous-energy, generalized-geometry, time-dependent code designed to track 37 particle types over broad range of energies” [19]. As such, the code is used for radiation transport, instrument design, shielding, safeguards, and other

radiation related fields. Unlike other radiation transport software, MCNP is the product of using statistical sampling through monte-carlo models along with multiple nuclear and atomic databases to produce a statistically valid response to radiation in each system. The use of Monte-Carlo simulating interactions and paths for particles through statistical means is the backbone of MCNP. Fundamentally, MCNP uses randomness and probability distributions to model individual probabilistic events for each particle emitted from a source.

1.7.1 MCNP Input File

An MCNP input file is composed of three sections, each separated by a blank line, historically referred to as cards due to the use of data cards in the initial development of the code. For ease of understanding, one should start by understanding the second of the three cards, called the surfaces card. In the surfaces card, all the surfaces to the geometry are stated. Surfaces may be understood as simple geometric 2D surfaces or borders that are built upon to design more complex structures for the modeled geometry.

The first card of the file is known as the cells card, which uses unions and intersections to construct complicated surface areas with the given surfaces in the second card. These surface areas may be correlated with others and thus create a body/volume. Critical information is also listed in the cells, such as the material that composes the cell and the density (in case the same material may be present with different densities). An additional vital part of the cells is designating the importance to a particle type. This importance lets the code know which particle type is to be tracked in each cell. This is to be specified since it may not be computationally efficient to model particle interactions in each surface given, and it is used to terminate the

particle once it has traveled past a distance where it would not be probable that the particle would travel back to the geometry in question.

The last section of the MCNP input file is the materials/data card. All material compositions are listed by a material identification number and their isotopic or atomic ratios. The data from this section is referenced back in the cells where each cell is assigned a material. Along with the materials, the card should also include the source specifications as well as the tallies. Dependent on the source and the type of particle tracked, the source specifications generally consist of describing the source as a volume or point source, energy spectrum of the particle emitted, the probability spectrum, and a description of the emission density in the volume or point source. Tallies in an MCNP input file are described as a counter which is used to count particle interactions at a place in the system. Tallies may be used to count particle interactions, particle fluence, energy fluence, or pulse. The geometry of the tally may be assigned to a cell, a surface or as a ring/point detector. Lastly, the card should state what mode it is (what particle to model and track) and the number of n-particles to model the physics. The cutoff for the number of particles generated from the source is referred to as “nps”.

These are the basic concepts and trivial sections of an MCNP input file, however there are more functions and additional details that can be included. More of these functions will be specified in the experimental section. After MCNP has ended its run, the software provides an output file listing many tables of information which can be used to determine the precision of the model, realism of the simulations, and reports the quantities of interest (tallies) and their statistical precision. An additional statistical checks table is provided in the output file with ten pass/fail tests done to better assess the simulation.

1.8 **Literature Background**

Neutron activation experimentation has been largely researched with the goals of neutron fluence quantification or trace analysis. Due to NAA's simplicity, any variety of methods and materials may be used to produce activation products. Neutron activation consists of a neutron source and a target, any variation of these two components will affect the activation rate. Multiple works of NAA were referenced for procedural and analysis methodologies and are described in the sections below.

The Idaho National Laboratory published a report, *Determination of the Deuterium-Tritium (D-T) Generator Neutron Flux using Multi-foil Neutron Activation Analysis Method* by D. Lee et al. As the title insinuates, the study utilized a D-T neutron generator that was used to activate a large number of foils of multiple metals with threshold activation cross-sections. The activated foils were then measured with a HPGe, a plastic scintillator, and a He-3 detector. Spectral peak analysis was then performed to determine the neutron flux from the generator [20].

Another related NAA work read for this thesis report was *Elemental Investigation of (Al-Cu) Alloys and Geological Samples Using Neutron Activation and XRF Analysis Techniques* by Essam Abd-Elhady Mohamed Hammad. Trace analysis of iron ore and Al-Cu alloys samples were carried out with an HPGe and x-ray fluorescence. A research reactor was used to irradiate the samples and measured their decay to determine elemental concentrations [21].

In similarity to the work done in this thesis, the work by Ahmet Ilker Topuz and Iskender Atilla Reyhancan *Neutronic Analysis of a Nuclear-Chicago NH3 Neuron Howitzer* and *3D Surface Radiation Dosimetry of a Nuclear-Chicago NH3 Neutron Howitzer* models a PuBe source in a Neutron Howitzer NH3 in MCNP. The results of the simulation were used to determine the ratio of collided to un-collided neutron flux in the drum and the estimated energy fluence per axial distance in the drum [22]. Neutron and gamma surface leakage from the drum was also determined from the MCNP simulation as Equivalent dose rates [23].

The last document used as reference to the thesis scope was *Neutron Flux Energy Characterization of a Plutonium-Beryllium Isotopic Neutron Source By Monte-Carlo Simulation With Verification By Neutron Activation Analysis* by Zachary Harvey. In the work done by Harvey, the neutron energy fluence of a PuBe source in a moderating drum was quantified using foil activation and MCNP simulations. The comparison of the fluences calculated from NAA and MCNP resulted in agreement at high energies but divergence at slower energies [24].

1.9 **Objective of Research**

The thesis work performed consisted of three parts, all with the goal of verifying and conducting NAA at Colorado State University. The thermal and resonance neutron energy fluence of two PuBe sources were quantified using NAA in two separate moderation setups. In the first part of the work, a Neutron Howitzer containing the 5 Ci source was modeled using MCNP. Neutron interactions were then simulated in MCNP with multiple foils in the sample channel to quantify the expected neutron fluences at each foil position. For comparison, the

second part of the work focused on foil activated in the Neutron Howitzer drum by irradiating them up to the point of measurable activity. The foil material and position were reproduced to match the MCNP simulation. An HPGe detector was used to measure the activity of the foils. The results of NAA were then used to calculate neutron energy fluence in the sample channels.

The final part of the thesis work consisted of the construction of a water moderated system for neutron activation. A water tank was constructed from multiple clear acrylic sheets to provide a visual of a sample in approximation to the source. This tank will house a 12 Ci PuBe source. The addition of the water tank will provide a new system to reproduce the work done in this report.

CHAPTER 2: MATERIALS AND METHODS

2.1 **MCNP Simulation**

To model the behavior of neutrons from the 5 Ci PuBe source, four separate versions of MCNP input files were constructed to model different setups. All the files share the same model geometry of the Neutron Howitzer drum constructed using the dimensions and characteristics listed in Table 5. The differences in the models pertain to geometric and material differences in the sample channels and will be specified later in this section. The cell and surface cards describe the universe of the model as a cylindrical volume 12 m tall with a radius of 45 cm. The dimensions of the universe were chosen to provide sufficient space for the drum. Since the purpose of the models only pertains to the behavior of neutrons in the sample channel, no geometry outside of the drum (room, floor, etc.) was included. The geometry of the drum consists of an aluminum drum shell filled with paraffin. Two source storage channels penetrate the top of the drum and are lined with aluminum. At the center of the drum is the source channel which is designed as a Plexiglas rod with an opening at the inner end used to contain the source. The rod is lifted to its exposed position which lines up the center of the source with the center of the sample channels. For simplicity, only one of the sample channels was modeled since any difference in neutron behavior from the second sample channel was assumed to be negligible. Additionally, to reduce the geometry in the model, the sample channel is lined with Plexiglas and only contains the plastic plug at the inner end of the channel. Any gaps in the drum such as gaps between the source rod to the source and free space in the sample channel were filled with air.

Most of the materials used for the MCNP model were sourced from the Compendium of Material Composition Data for Radiation Transport Modeling by PNNL [25]. Material

compositions making up the geometry are aluminum, paraffin #396, dry air, 3:22 ratio PuBe, stainless steel 316 #333, plexiglas (polymethyl methacrylate), plastic (polyethylene non-borated) #275, as well as natural aluminum, gold, indium, scandium, and iron. The composition of the PuBe source was directly source from another work, C. T. Nguyen, "Verification of the content, isotopic composition and age of plutonium in 19 Pu-Be neutron sources by gamma-spectroscopy", which looked at determining the isotopic composition of PuBe sources [26]. For the purpose of these models, the isotopic composition of the source is only relevant if it effects neutron scattering and self-attenuation. As little is recorded for the source modeled, assumptions were made regarding the Pu to Be ratio and so, the intensity neutron yield of the source will be affected.

In addition to the materials, the last card contains the source specification card and the tallies. The simulation is instructed to produce neutrons up to 1E7 histories. The nps was determined based on the reported neutron activity of the sources as reported on the 5 Ci PuBe safety plan [17]. As previously discussed, the PuBe neutron energy spectrum used was provided from the IAEA Technical Report series 403, Compendium of Neutron Spectra and Detector Responses for Radiation Protection Purposes [27]. The technical report is composed of multiple energy spectra from multiple neutron sources gathered from different national laboratories. The spectrum used is listed on page 106 of the report [28]. The source definition card specified the positioning of the source and dimension vectors that describe the geometry of the source. As required for volumetric sources, the additional axial and extent parameters are included. A radial parameter is notated as -21 1 which is the built in power law function notation for linear radial sampling for a volumetrically uniform source. The extent parameter was described with 0 1 for uniform sampling. These parameters describe a uniform emission of neutrons from any point in

the volume source. Lastly, F4 or F5 tallies were designated to record the simulated fluences. An F4 tally measures the averaged fluence at a cell, while an F5 tally measures the fluence at a point detector (not a volume). These tallies record the average particle fluence in a cell, that is neutrons per cm^2. In addition to the tallies, energy bins are specified for each tally with the maximum energy bins of 0 eV, 0.025 eV, 0.5 eV, 3 eV, 10 eV, 1 keV, 5 keV, 10 keV, 100 keV, 1 MeV, 3 MeV, 5 MeV, 7 MeV, 10 MeV, 13 MeV, 15 MeV, and total fluence.

Listed below are the differences between the four versions in the MCNP input files modeled to characterize the neutron fluence in the drum. All these versions are identical except for what is listed. These first two versions of the input file were used to quantify a ratio of moderation between air and plastic moderation in the sample channel. This was done to provide more information on what the expected neutron energy fluence spectrum is in the most basic sample channel geometry. Versions 3 of the input files were used in comparison to the foil activation procedure in the Neutron Howitzer.

1- The sample channel is filled with air that is sectioned in volumes 2 cm thick. Each air volume was tallied.
2- Same as version 1 except the channel is filled with plastic instead of air.
3- A total of 6 input files, each modeling a foil made of one gold or indium. Each foil was positioned directly in front of the inner sampling area of the channel, 4 cm from the front of the area, and 8 cm from the front. Each foil position includes four 4 cm thick plastic spacers that fill the sample channel to the spring (spring not modeled).

2.2 **Foil Activation Procedure**

In preparation for the procedure, theoretical calculations of activity had to be preformed to determine an approximation of counting times and irradiation times for each foil. To accomplish the required calculations two highly conservative assumptions were made. It was first estimated that the neutron fluence (from the safety plan) is 1E5 n/s cm^{-2}. Then, in the most ideal scenario with 100% moderation and foil activation per neutron the thermal neuron fluence is 1E5 n/s cm^{-2}. Using this value, Equation 3 was used to calculate the saturated activity for each foil based on their average foil material mass. Once the saturated activity was calculated, it was inserted into Equation 4 to calculate the estimated activity after time t irradiated. Due to the nature of an exponential function, solving for the time at which the saturated activity reaches 100% is not possible, and so to simplify, the activity required was reduced to 0.99 SA. Hence, Equation 6 calculates the time required for 99% of saturated activity. Once an approximated irradiation time was calculated for each foil, the expected activity per foil was recalculated to verify the activation results. Notably, some of the calculated irradiation times were extremely long with low final activity. For practicality, the irradiation times were truncated to more reasonable times taking into account the lower activity that would be achieved. Nevertheless, these initial time calculations were used as an initial estimation of the magnitude of time required for each foil material (minutes, hours, days). Ultimately, practicality determined the final irradiation times for the foils.

Based on the calculated theoretical activities, Equation 7 was used to calculate the maximum counting time for each foil material. The equation was used to give a representative time scale needed for most of the activity in the foils to decay. As a conservative parameter, the theoretical detector efficiency was designated to be 1%. Once again, practicality and procedural

efficiency were considered when determining the maximum counting times. All the proposed irradiation and counting times measured are listed in Table 7.

$$t_{irr} = \frac{-\ln(0.01)}{\lambda} \quad \text{(Equation 6)}$$

Where λ = decay constant (1/hour).

$$t_m = -\ln\left(1 - \frac{(0.99\, MaxCounts)\lambda}{\phi Y \varepsilon}\right) \quad \text{(Equation 7)}$$

Where λ = decay constant (1/hour),

Max Counts = maximum number of counts desired to measure,

ϕ = neutron energy fluence (n/cm^{2}s),

ε = detector efficiency.

Table 7: Proposed foil irradiation and counting times for each material. Resultant count and irradiation times for each foil is recorded in Appendix III.

Foil Element	**Irradiation Time (h)**	**Counting Time (h)**
Au	96	6
In	6	12

In preparation for irradiation, every foil was marked with its designator ID on one face of the foil. Pictures of the foil kit and the foils used are shown in Figures 5 and 6. An energy

calibration curve was produced for each detector by measuring the photopeaks from Cs-137, Co-60, Ba-133, and Mn-54 sealed calibration sources manufactured by Eckert & Ziegler Analytics. The same photopeaks were measured to calculate the detector efficiency using Equation 5.

Figure 5: Activation foil kit used for NAA.

Fugure 6: Gold foil used in NAA of 1 cm diameter and Cd covering.

To measure background activity, one foil of every metal type was counted on an HPGe in intervals until the maximum counting time was reached. To maintain the closest possible geometry, all foils were counted centered to the detector with the ID marker facing up towards the sliding lid of the lead shield. Each spectrum was saved and analyzed for any peaks using Genie-2000. After measuring background counts, two gold foils (A and B) were placed in each sample channel, in each corresponding position sandwiched by the plastic spacers in the sample area. It was assured that each foil ID marker coincided with the position designation and the marker was facing towards the outside of the drum. To ensure that the foil was secure at the

center of the channel, additional plastic spacers were added at the end of the channel. Based on the calculated times in Table 7, the gold foils were exposed to the source (lifting the source rod to initiate exposure). After exposure, each foil was immediately taken to be counted on an HPGe, with the ID marker facing up. The two HPGe detectors used had model numbers GEM-35190-S operating with a bias voltage of 3.5 kV and are nicknamed Joliot and Curie with serial numbers 40-TP40990A and 40-TP40990A respectively. The time elapsed after the lowering of the source to stop the irradiation and starting the sample counting was recorded for each foil. The irradiation time was measured to the minute while transfer and count time were measured to the second. Additionally, each foil was measured in the same detector used for measuring the foil's background. The spectrums were monitored until a desired photopeak area count for each photopeak was reached. Based on the background intervals measured, the count time was adjusted to match the closest background spectrum count time. This was only done for one of the foils, as the other foils of same material will be set to count for the same time as the initial foil.

Next, gold foils C and D were prepared for irradiation. Foil D was encased in the cadmium covering before inserting into the sample channel. In the same fashion as before, the foils were placed in their corresponding positions with the ID marker facing out. After irradiation, the foil was removed from the drum, removed from the cadmium casing, and counted on the HPGe following the same procedure as the other foils. All relevant times were recorded for these foils. Another background spectrum was measured for foils B and C, and they were exposed again in their corresponding positions with Cd covering. Likewise, these foils were irradiated, transferred and their spectrum was recorded. Thus, six irradiation spectra were recorded from Au foils, three of bare foils, three of Cd covered foils, and two at each position along the sample port. For each spectrum, the Genie 2000 software was used to detect

photopeaks, determine photopeak counts, correct for background, and provide the efficiency for each peak.

The same procedure above was repeated for all In, foils. In average, 4.3 minutes was the transport time for the activated foils with the exclusion of gold foil C's extensive time due to user error. Each foil is listed on Table 8 with their ID letter and positioning along the sample channel, as well as the repeated foils with Cd covering however a more detailed listing of the irradiations is recorded in Appendix III, along with an example of a measured gamma energy spectra. After Irradiation, each foil was properly stored in its packaging and stored away in the laboratory for the continual decay of activation products.

Table 8: Foil's ID letter and position for each material in NAA procedure.

Foil Element	**Cd**	**Foil ID**	**Position in Channel (cm)**
Au	No	A	0
	No	B	4
	No	C	8
	Yes	D	0
	Yes	B	4
	Yes	C	8
In	No	V	0
	No	W	4
	Yes	Y	0
	Yes	X	4

2.3 **Water Tank**

2.3.1 Tank Construction

Due to the nature of neutrons, determining appropriate shielding thickness is a complicated task that becomes more complicated when the neutron energy is not discrete. To reduce uncertainty in shielding calculations, such as the diffusion lengths, an MCNP model was used to determine appropriate water shielding for a 1 Ci PuBe source.

A simple MCNP input file was constructed which described a cylindrical surface with a height of 150 cm and a radius of 70 cm. The inner volume declared the universe boundary for the model, where any neutrons traveling outside the cylinder volume were terminated. The universe volume was then filled with air. At the center of the universe a series of planes were designed to construct a 60 cm cube filled with water. No additional geometry was described in the model. The source specification card described the source as a point located at the origin of the tank. A visual of the water cube model is shown in Figure 7. The same energy yield spectra used for the Howitzer drum model was used for the energy parameter. A series of F5 point detector tallies were positioned at x=5 cm, y=0 cm, z=0 cm and increased in the x position by 5 cm until reaching 60 cm. Due to the source containing 1 Ci or activity, the nps was set to 2E6 histories (safety plan). After running the MCNP input file, all the tally results were un-normalized by the nps and the fluence per hour was calculated. Using the hourly fluence rates the number of neutrons passing each shielding thickness was calculated for each tally point. This calculation was done to provide several possible neutron exposures from one surface of the cube assuming an 8-hour long exposure next to the cube surface. The scenario described is unlikely to occur since any use of the tank with the source does not require continuous monitoring, however the calculation was done to assure an over exposure to neutrons from the tank is unlikely to occur.

The results of these tallies and calculations are listed on Table 9 with the additional results from an 8-hour neutron count for each face (cube face was calculated from the water thickness) at each thickness and the reduced intensity of 5 MeV gammas which are the average energy gammas emitted from a PuBe source [29]. The intensity reduction of gamma rays through a mass is given by Equation 8. Where the attenuation coefficient for 5 MeV gammas in liquid water was sourced from NIST Standard Reference Database 126 [30].

$$Intensity\ reduced = 1 - \frac{I}{I_o} = 1 - e^{-\mu * x} \qquad \text{(Equation 8)}$$

Where I = Remaining Intensity,

I_o = Original Intensity,

μ = attenuation coefficient (cm^{-1}),

x = Mass Thickness (cm)

Table 9: Results from MCNP water cube model. The table lists the neutron fluence at each tally and its error, the expected 8-hour neutron exposure at a cube face, and the expected gamma intensity reduction at each water thickness. Based on the results, a water thickness of 40 cm was determined to be the most fitting.

Water Thickness (cm)	8 hr Neutrons Incident per Face	Gamma Intensity Reduction (%)
5.00	1.41E+10 ± 25.1%	14.06
10.00	7.92E+08 ± 21.9%	26.15
15.00	4.05E+07 ± 73.6%	36.53
20.00	2.78E+05 ± 28.3%	45.46
25.00	1.51E+04 ± 23.2%	53.123
30.00	1.25E+03 ± 18.8%	59.72
35.00	1.55E+02 ± 18.1%	65.38
40.00	2.61E+01 ± 20.6%	70.25
45.00	5.24E+00 ± 22.8%	74.44
50.00	1.15E+00 ± 24.0%	78.03
55.00	2.67E-01 ± 24.3%	81.12
60.00	6.33E-02 ± 24.1%	83.77

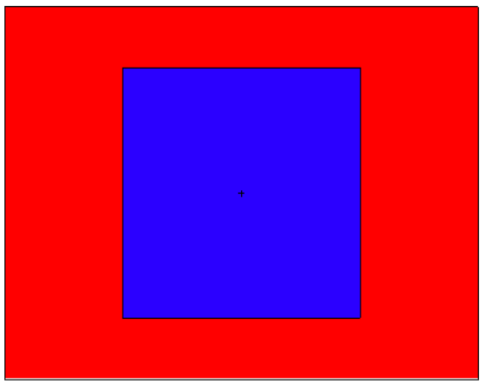

Figure 7: ZX planar view of MCNP water cube model where the red is the universe filled with air, the blue is the water cube, and the white is the void.

Based on the values reported in Table 9, it was determined that a water thickness from the source of 40 cm had the best combination of 8-hour neutron exposure (~27 neutrons per face) and gamma intensity reduction (70%) for the construction of the water moderating tank. Once a proper water thickness was found for the tank, a tank configuration paralleling the construction of the neutron Howitzer was designed. A schematic illustration of the initial tank design is shown in Figure 8. Key characteristics of the 80 cm cube tank are four sample channels, one on each side face, with a sample drawer that can be inserted or removed for sample placement. A source insertion port at the center of the tank where the source may be lowered to the level of sample channels, where their inner ends are at an equal distance from the source. The source port is capped at a lower depth than the sample channels. Allowing for the source to be rested on the bottom of the port for short-period storage.

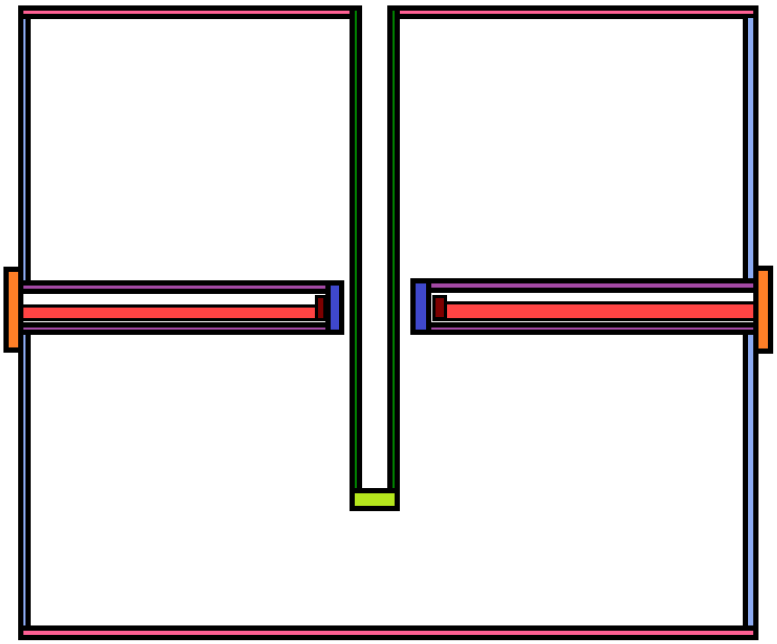

Figure 8: Illustration of all components needed for the design and construction of water filled.

A total of six sheets of acrylic were purchased with dimensions of 32 inches by 48 inches as offered by the manufacturer. The sheets were colorless and were used to make up the main body of the tank. Based on the recommendations given in a tank building guide published by Professional Plastics and the tools available for the project, a thickness of 0.5 inches was chosen for the main body of the tank [31]. Three different diameter acrylic pipes, 2.875 inches, 2.375 inches, and 1.315 inches were also purchased for the sample channel, sample drawer, and source port respectively. An additional smaller sheet of 0.125-inch-thick acrylic was purchased for the end caps of each pipe and other smaller parts needed. Lastly, Weld-On 4 and 16, acrylic solvents, were acquired to adhere the acrylic components together and form a solid tank.

First, all the 0.5-inch acrylic sheets were cut to size (32 in x 32 in) using a table saw. Multiple 6-inch squares were cut to act as braces on the inner and outer intersection of the sample channels to reduce any stresses on the pipe and provide a larger surface area to secure the pipes through the sheet. Multiple squares were then cut as end caps of each intruding pipe. All the pipes were cut to their corresponding lengths. Lastly, circular holes were drilled out of four of the face sheets where the sample channel pipe was to be inserted. A significant amount of trial and error occurred while preparing each component piece to find which cutting method worked best on acrylic given the tools available.

Once all the components were prepared and precut, the construction of the tank began by adhering all the side sheets together, then attaching the bottom sheet to construct an open-faced cube. All the end caps were then glued to their corresponding sample channel pipes and source pipe. The end caps were then trimmed to not protrude past the diameter of the pipe. Once the pipes were prepared, they were attached to the tank where the side sheets were sandwiched between two braces. This completed most of the tanks' main body. The construction of the

sample drawers consisted of cutting the corresponding pipes in half, to create semi-cylinders. Next, the end caps were glued to the drawer, where the inner end cap was trimmed to match the drawer as a semi-circle and the outer cap was cut as a large 6-inch square of 0.5-inch thickness. This outer end cap provides a large grip area of the drawer for each use and adds neutron shielding from neutrons tunneling out the sample channel. Lastly, the source pipe had an end cap attached and trimmed. The pipe was then adhered to the last sheet of acrylic and the two braces. Once all the internal components of the tank were complete and secured, as well as the lid of the tank and the source pipe, the tank was sealed by adhering the lid to the tank. The final seal was allowed to cure for multiple days to allow the pieces to fully harden before transporting to their final designation. Figures 9-12 show pictures of the assembly and acrylic welding process.

Figure 9: Gluing acrylic sheets together to form the main body of the tank.

Figure 10: Leak testing tank full of water before adhering top sheet on tank. After letting the full tank rest for a couple of days, all joints and edges were checked for leakage. No deformations or leaks were spotted.

Figure 11: cementing the top sheet to rest of tank (tank is laying upside down on top of sheet.

Figure 12: Final additions to tank were completed and protective film removed from the main body.

CHAPTER 3: RESULTS & DISCUSSION

3.1 MCNP Data Analysis

The MCNP results from each run were compiled and organized by their foil material and position. The reported fluence and error given by MCNP is normalized by the number of histories simulated, thus un-normalizing the given values will produce the simulated neutron fluences per energy in each foil material. The MCNP output file for each foil simulation passed all ten MCNP statistical checks. The un-normalization of the simulated fluences in plastic and air-filled sample channels were calculated, with no more than three of ten checks failing the statistical checks for a minority of the tallies. This may be due to the repeated F5 tallies used.

The comparison of MCNP results with filled sample channels are shown in the Figure 13, where the first set of plots illustrates the comparison between the moderating materials and the magnitude of each energy neutron fluence simulated at every 2 cm position in the sample channel. The decrease of every fluence energy shows an exponential decay with respect to the distance from the source. As expected, the simulated fluences decrease along with the neutron energy, maintaining a continual majority of neutrons in the thermal or resonance energy range. As described in the background sections, this is caused by the continual moderation of higher energy neutrons into lower energies. All these trends are present in both air and plastic filled sample channels and foil simulations. For further comparison, Figure 14 shows the same results from MCNP as scattered plots, with an exponential curve fitted to the plastic and air moderation set. Additionally, an effective curve has been added to the set which is the mathematical average of both sets of moderation curves. These effective curves serve as a baseline expected neutron fluence at any position along the sample chamber independent from the spacer/moderator plastic

cylinder arrangements around the sample. The effective curves shown in the graphs are $y=12035e^{-0.176x}$ and $y=69759e^{-0.17x}$ for thermal neutron fluence and total neutron fluence respectively.

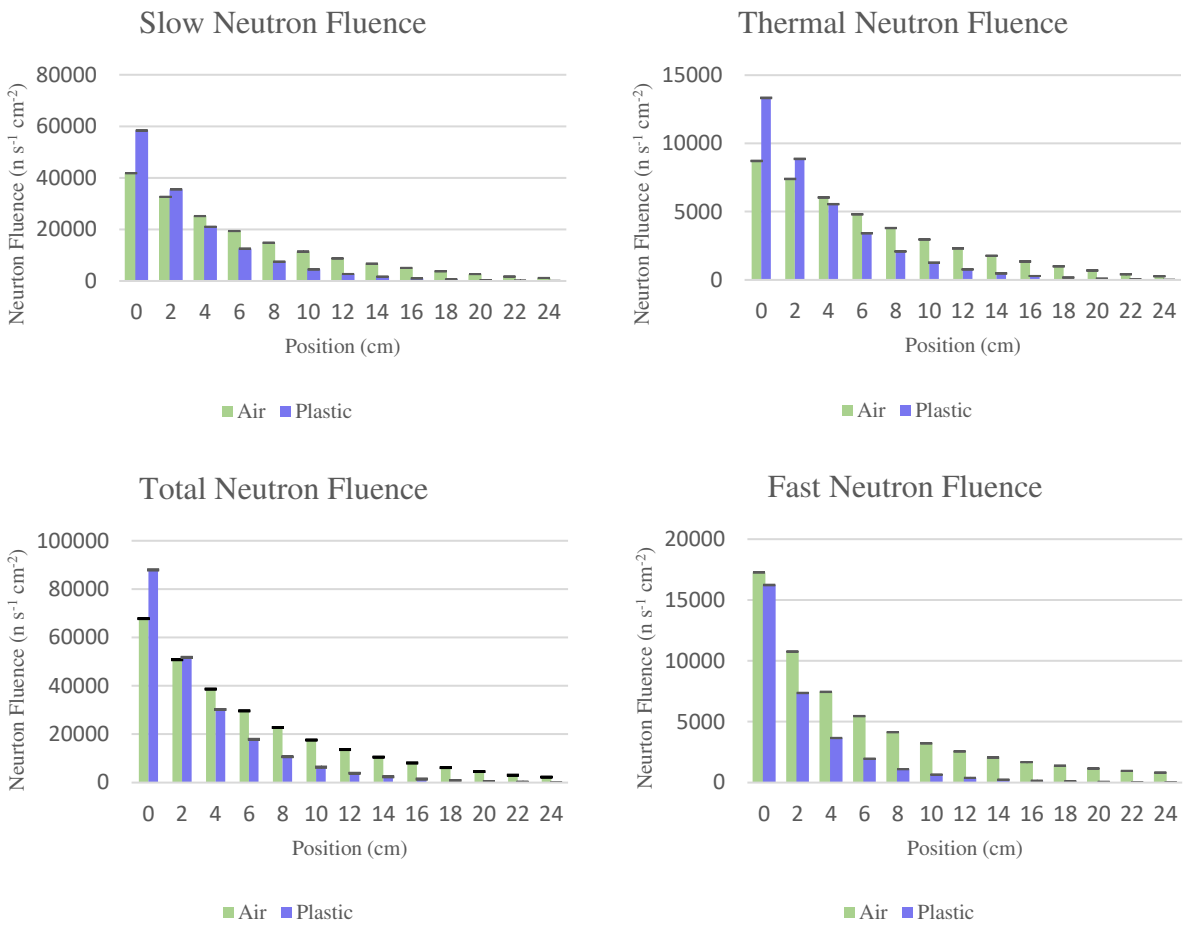

Figure 13: MCNP simulated neutron energy fluence in sample channels filled with air or plastic.

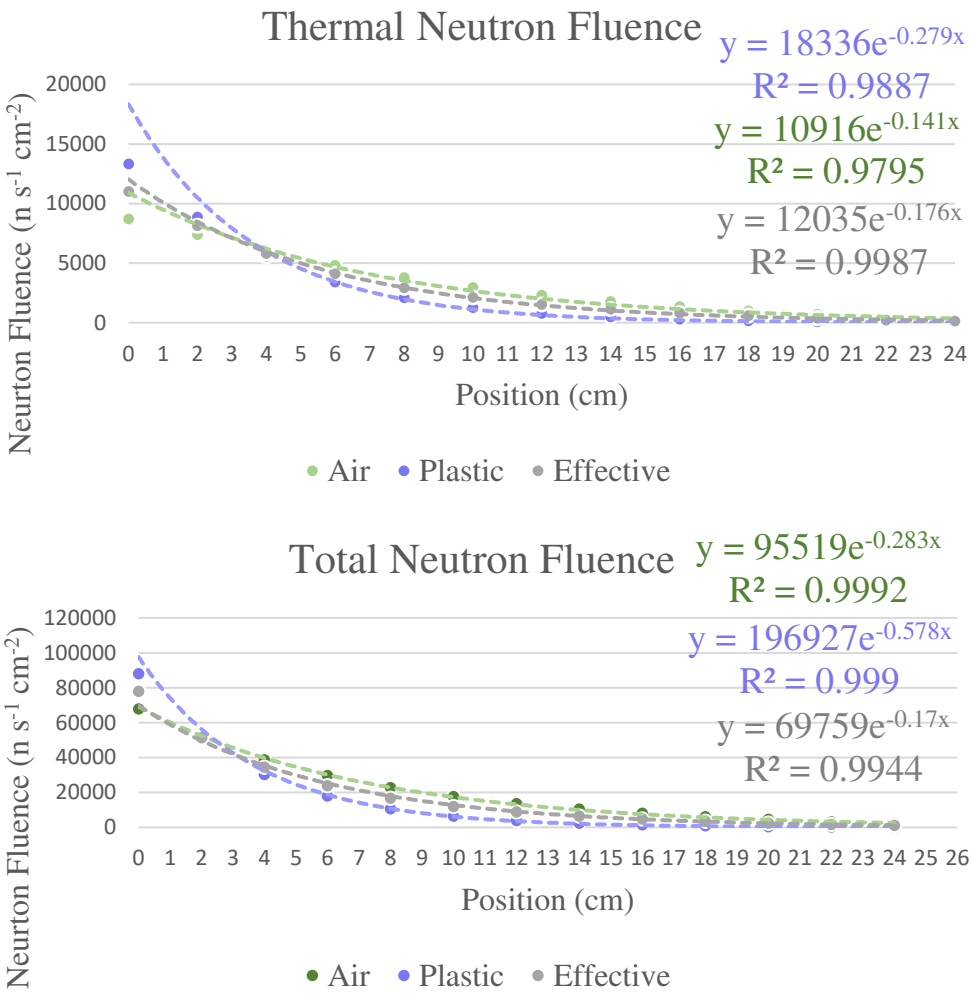

Figure 14: Graphed results of MCNP simulated neuron fluences in sample channels filled with air or plastic for thermal energy neutrons and total neutrons. Each graph is fitted with an exponential curve for the results from air or plastic moderation and an effective curve based on the average of both sets of results.

Figure 15 shows the results of the foil MCNP runs. The simulations which contained materials with a large molar mass, such as gold, and indium resulted in lower thermal and resonance neutron fluences when compared to lighter material such as Al. This is due to the F4 tally recording the average neutron fluence in the foil and the neutrons behaving differently in heavy molar materials than in lighter materials.

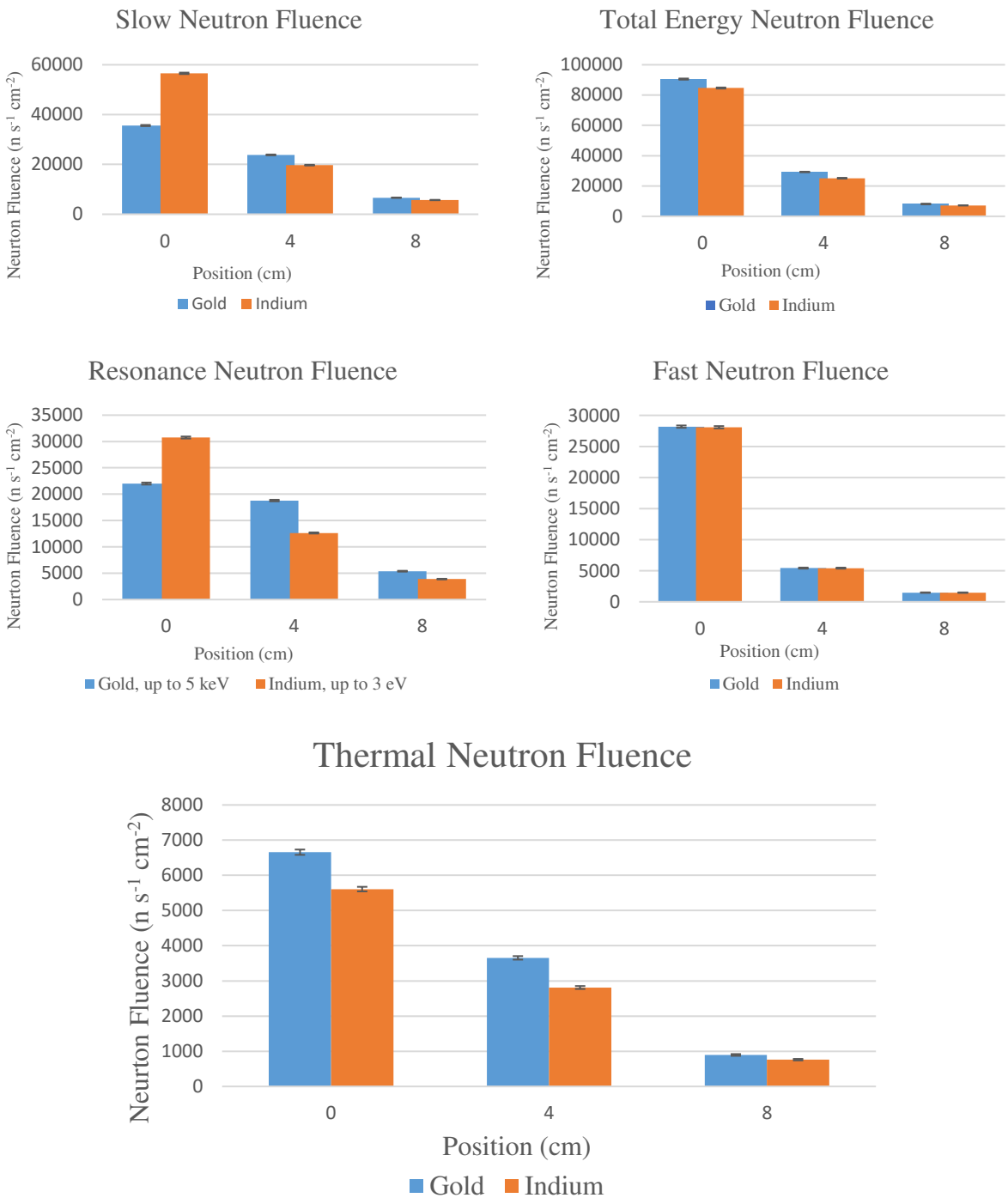

Figure 15: MCNP modeling of neutron energy fluences for Au and In foils in positions 0 cm, 4cm, and 8 cm.

3.2 **NAA Results & Comparison**

After the foil activation and analysis of the spectra, the calculations for thermal and resonance neutron fluences were calculated by comparing the net counts of each photopeak, with and without Cd recorded at a given position. Using the difference in the activation from the bare foil and the Cd covered foil, the amount of activation produced from resonance neutrons was calculated. Once the activation from resonance and thermal neutrons had been differentiated, the fluences for thermal and resonance neutrons at each position was derived. Equation 9 shown below is the rearrangement of Equation 4, but it has been modified to include counts measured (instead of induced activity), the photopeak detector efficiency, and decay corrections. Thus, the equation can calculate i energy fluence (ϕ_i) given recorded net j energy photopeak area counts. And so, having calculated both thermal activation counts and resonance activation counts, the thermal and resonance neutron fluences were calculated for each position.

$$\phi_i = \frac{\lambda(C_j)}{N_t \varepsilon_j \, \sigma_i \Gamma_j (1-e^{-\lambda t_{irr}})(1-e^{-\lambda t_{count}})(e^{-\lambda t_{tran}})} \qquad \text{(Equation 9)}$$

Where λ = decay constant (1/s),

C_j = Net area counts for j energy photopeak,

N_t = number of target atoms in foil,

ε = Detector efficiency at j energy,

σ_i = i energy neutron cross-section for target particle (cm^2),

Γ_j = branching ratio for j energy photopeak,

t_{irr} = irradiation time (s),

t_{count} = detector count time (s),

t_{tran} = transfer time (s).

Additionally, the activity induced from slow neurons (activity from thermal and resonance neutrons) and fast neutrons was calculated along with the cadmium ratio, and slow/fast activation ratio. All these values are shown in Table 10. Note that there is no activation occurring in the Au foils from fast neutrons since the cross-section for higher energies remains near zero. Figures 16 to 20 show the plotted NAA results and the comparison of both sets of results to MCNP results.

Table 10: NAA Results from Au and In foils at 0 cm, 4 cm, and 8 cm along the sample channel. Listed are the calculated thermal fluence, resonance fluence, activity induced, cadmium ratio, and their relative uncertainties.

	Position (cm)	φ Thermal	φ Resonance	Activity (Slow, Bq)	Activity (Fast, Bq)	Cd Ratio
Au	0	3.12E4± 3.06%	6.51E2 ± 3.76%	1.51E3 ± 1.40%	0.0	3.02 ± 3.84%
	4	2.52E4 ± 0.11%	1.68E2 ± 2.29%	1.01E3 ± 1.12%	0.0	9.52 ± 2.11%
	8	2.73E4 ± 0.11%	5.59E1 ± 2.23%	1.04E3 ± 1.83%	0.0	1.03 ± 2.90%
In	0	9.38E4 ± 1.38%	7.97E2 ± 1.74%	1.32E4 ± 1.03%	3.47± 5.45%	7.38± 1.54%
	4	7.73E4 ± 1.66%	3.64E2 ± 1.96%	1.02E4 ± 0.98%	9.49E-1 ± 16.5%	1.29E1 ± 1.81%
	8	4.63E3 ± 5.85%	2.05E2 ± 4.57%	1.58E3 ± 1.02%	2.73± 5.36%	1.81 ± 8.37%

Based on Figures 16, it is seen that the highest neutron fluence is between 0 cm and 4 cm, and exponentially decreases along the sample channel. While the largest thermal fluence is at position 0 cm, the largest ratio of thermal to resonance neutrons is observed at position 4 cm, as seen in Figure 17. This high CR position signifies that at 4 cm the sample will experience more thermal neutrons than resonance, which is ideal if thermal exposure is preferred. Another expected result is the largest activity from threshold neutrons occurring at 0 cm, where neutrons have experienced fewer interactions than deeper in the channel. The activation experienced by In from fast neutrons was much lower than the activation from slow neutrons due to their irradiation time. The lower activation from fast neutrons was observed since the irradiation times chosen for the foils was determined with saturation of thermal activation in mind. Based on the NAA results, the thermal neutron fluence is expected to be in the mid 10^4 range and high 10^2 resonance energy range, which is shown in Figures 19 and 20.

Figure 20 shows the results from MCNP and NAA. There is a significant difference between Au and In in thermal neutron fluence observed from NAA and MCNP datasets at each position, this indicates the composition of the sample itself may greatly influence the intensity of the fluence, even if the geometry of the sample is identical. The figure also includes the effective curve derived from the plastic and air channels, which falls in between NAA and MCNP datasets. Future irradiations with more diverse geometry may result in a different magnitude range of neutron fluences than what was observed in this work. Regardless, the work described in this report is to establish a baseline of expected neutron energy fluences to determine the best fitting exposure procedure for any given sample. The effective curve shows itself to be an appropriate model for the neutron Howitzer drum, with a thermal fluence of $y = 12035e^{-0.176x}$ and a total fluence of $y = 69759e^{-0.17x}$. Based on the effective curve, Equation 1 was used to calculate

the diffusion length of thermal neutrons in the Howitzer. Thus, a diffusion length of 5.88 cm may be used to calculate the intensity of the neutron fluence in the sample channel from the total energy spectrum, and a diffusion length of 5.681 cm for thermal neutrons only.

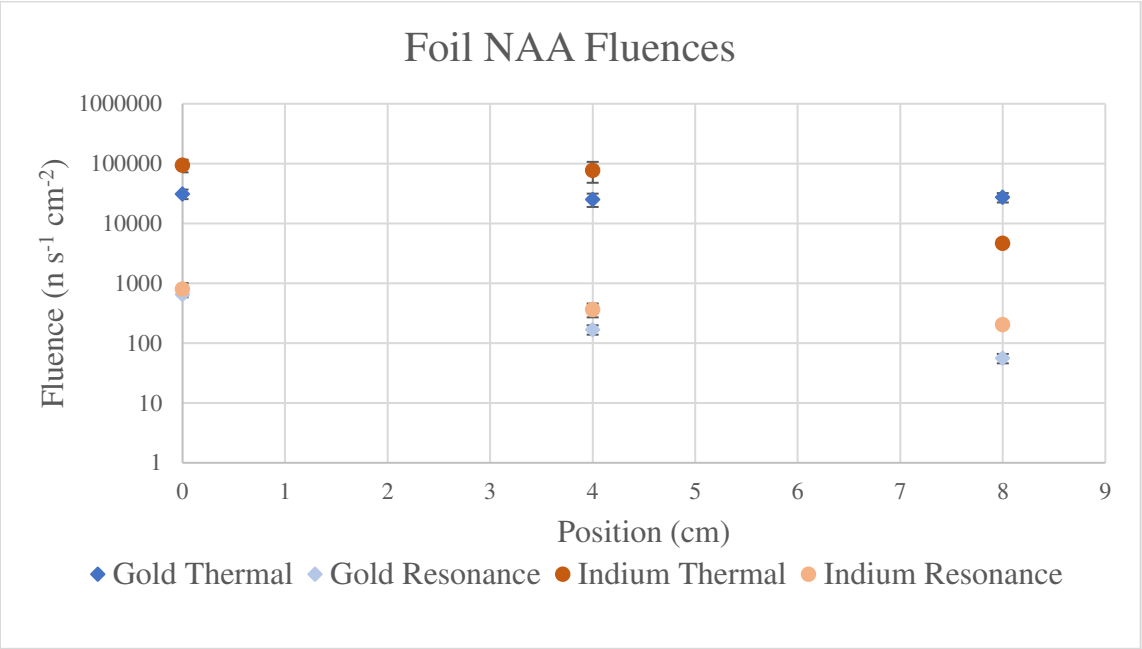

Figure 16: Plot of NAA results from Au and In foils.

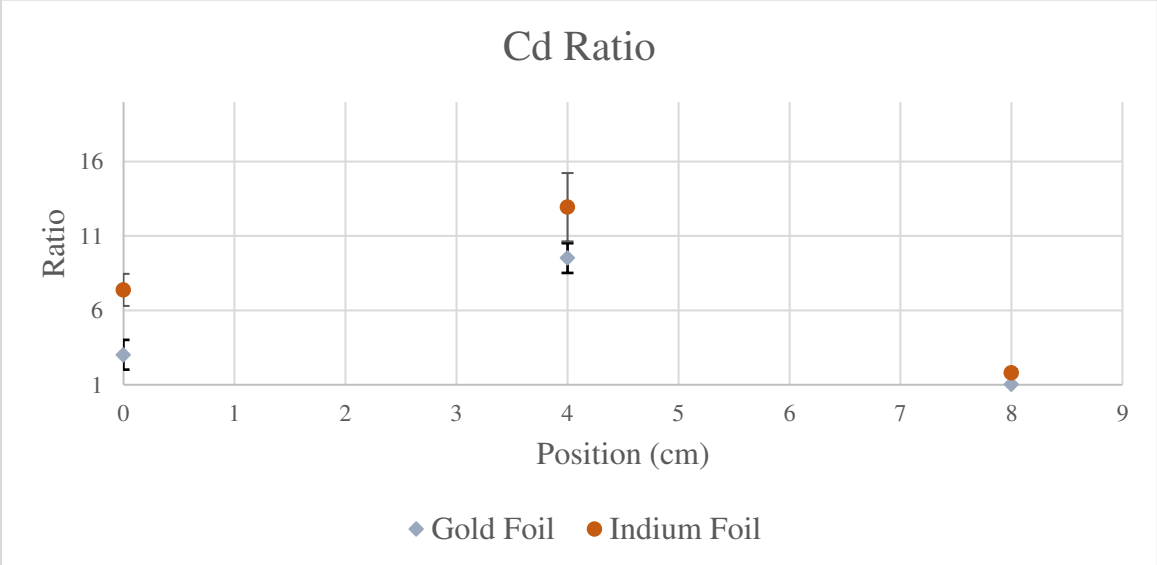

Figure 17: Cadmium ratios of Au and In at each position.

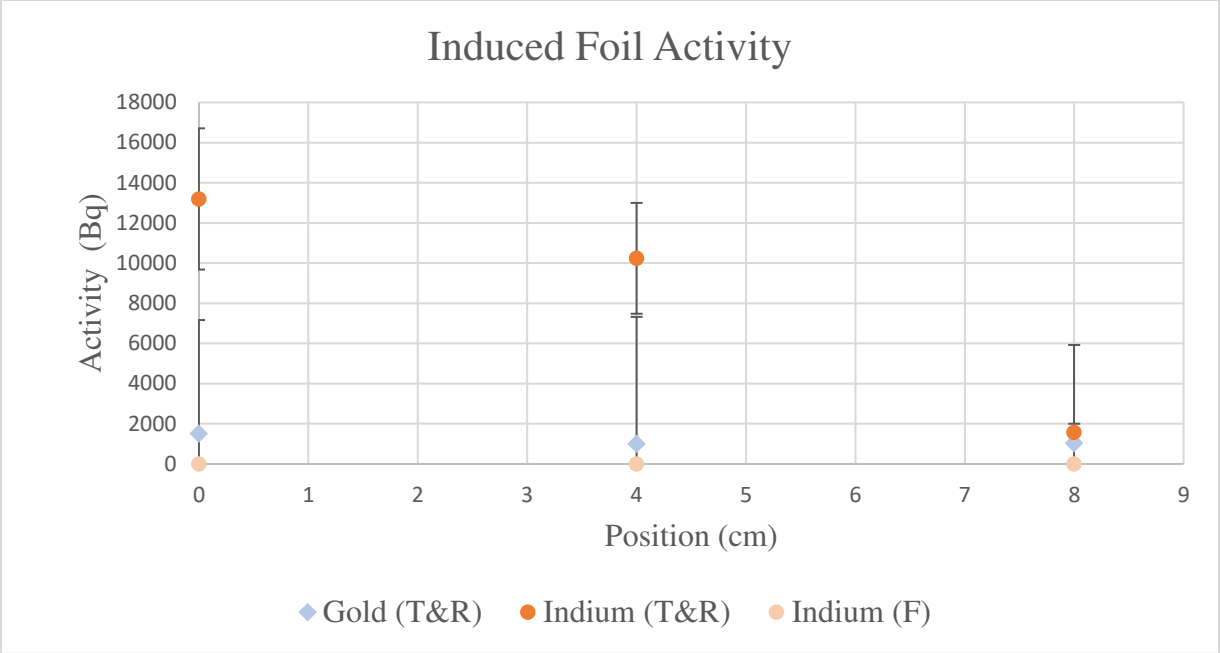

Figure 18: Plot of induced activity in each foil after irradiation from fast and slow neutrons.

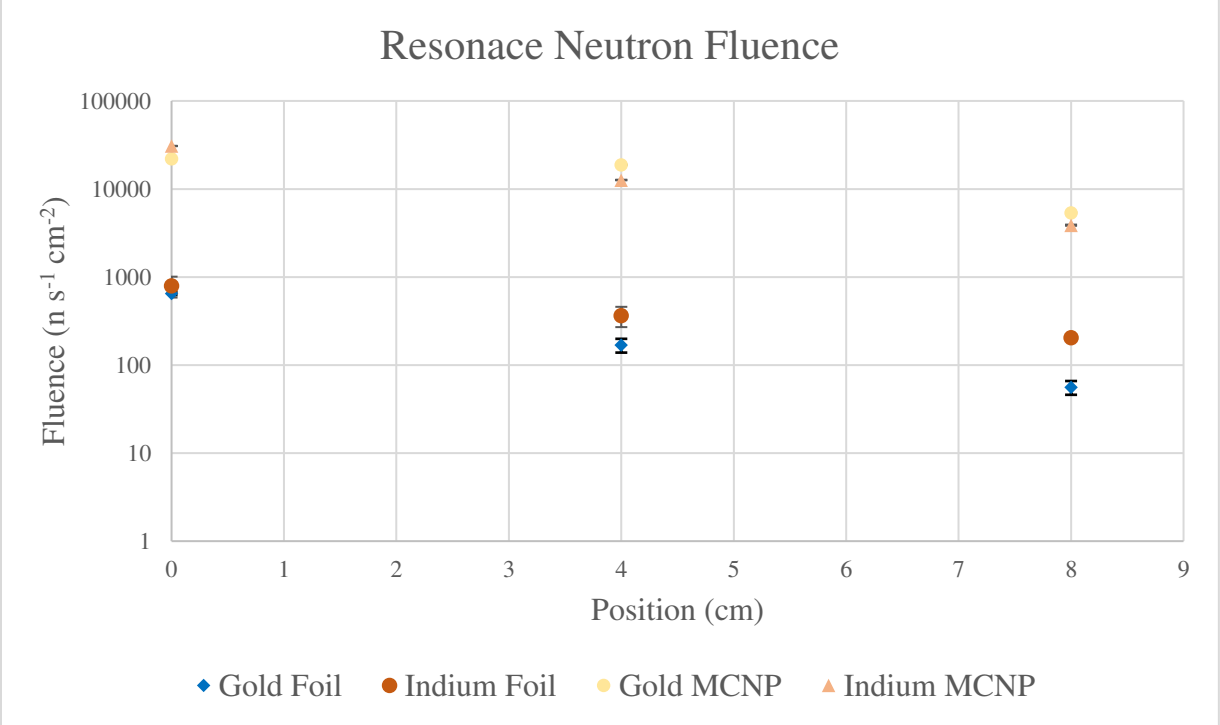

Figure 19: NAA derived resonance fluences (up to 5 keV for Au and 3 eV for In).

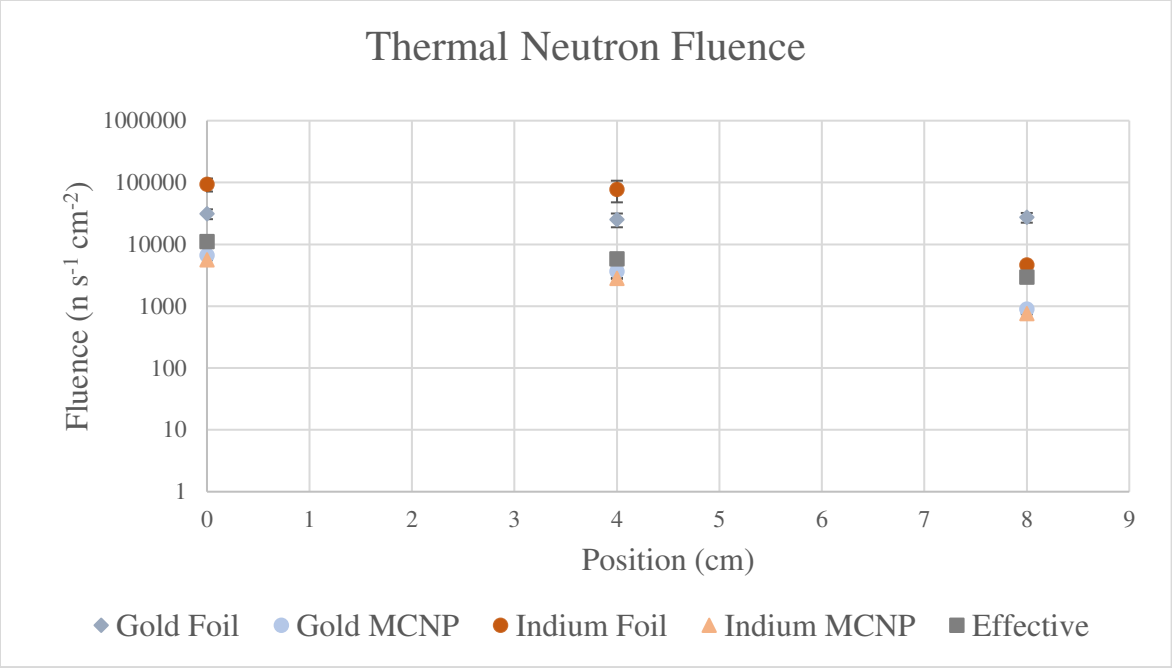

Figure 20: Plotted results from NAA and MCNP for thermal fluences and how they compare to the effective curve.

CHAPTER 4: UNCERTAINTY & ERROR ANALYSIS

4.1 MCNP Uncertainties

When comparing the results from the MCNP modeling to the NAA fluences (Figures 19 and 20) it is shown that the fluence recorded by MCNP is approximately an order of magnitude from those from NAA. When comparing the results for resonance neutrons, the fluence measured by MCNP is greater than the foils, however the opposite is observed for thermal neutron. This may be due to simplifications in the Howitzer model. A series of expected warnings were reported in the output for each file, such as high relative error in certain energy bins where the number of neutrons of that energy were too small for strong statistical significance. Regardless of all files passing the ten statistical checks, editing of the model and tally types will be needed to be done to reassure the simulation parallels NAA results and thus can be used to simulation dose rates or complex sample geometry irradiation scenarios.

4.2 Experimental Uncertainties

Uncertainty calculations for the experimental neutron fluences contained partial uncertainties from each individual detector efficiency at energy peak, net count uncertainties, branching ratio uncertainties, decay constant uncertainties, and the reported cross-section uncertainties. The neutron fluence experienced by the foils were also affected by uncertainties in irradiation time, transfer time, counting time, and the foil's mass. Due to the irradiation times being measured in the range of hours to days, the expected (but not measured) uncertainty from the irradiation times are within ±1 minute from the reported time as they were measured on a common clock. The transfer time from irradiation to detector was expected to be in the range of

minutes, so a hand-held timer was used which recorded in minutes and seconds. Due to reaction time and timer ease of access during transfer process, the uncertainty in the transfer time is conservatively assumed to be 3 seconds. Unlike the previously discussed measured times, counting time was tracked by the Genie-2000 software which measured the live and real counts times. The software reported measured times to the second of the preset count times. An additional source of uncertainty, which was not incorporated in the calculations, is due to any uncertainty in the reported foil masses from Shieldwerx. No scale calibration certificate was provided to determine an uncertainty in the reported masses of the foils and for ease of calculation, the reported masses were kept for the calculations.

Aside from the calculation uncertainties discussed above, geometric differences during exposure and counting could result in activation differences which could impede the direct comparison neutron fluences at each position. However, any millimeter difference in foil position from the center of both the detector and sample port (visual confirmation, not measured) is not expected to significantly affect the magnitude of activation product activities. If additional foils were to be irradiated for each position (more activation comparisons) then further parameters would need to be taken to assure consistent geometry, however such extents were not deemed necessary for the work described in this report.

CHAPTER 5: CONCLUSION

5.1 Summery

With the characterization of the thermal neutron fluence in the Neutron Howitzer through MCNP and NAA, an effective model of the neutron's behavior was developed to provide the intensity of thermal or total neutron fluence at any position along the sample channel. The neutron diffusion lengths for thermal and full spectrum neutron intensity in the sample channels were also derived based on the effective curves. It was also determined that sample composition and shape will greatly influence the neutron fluence along the channel. However, the effective model will provide a sufficient estimation of the minimal neutron fluence which may be used for future irradiations or NAA.

The completion of the water moderated tank for a lower activity PuBe source is an additional teaching tool for the program. The use of the tank for future labs will facilitate understanding the concepts of neutron activation by providing an easily accessible moderator. A finalized image of the tank in its final resting place is shown below in Figure 21:

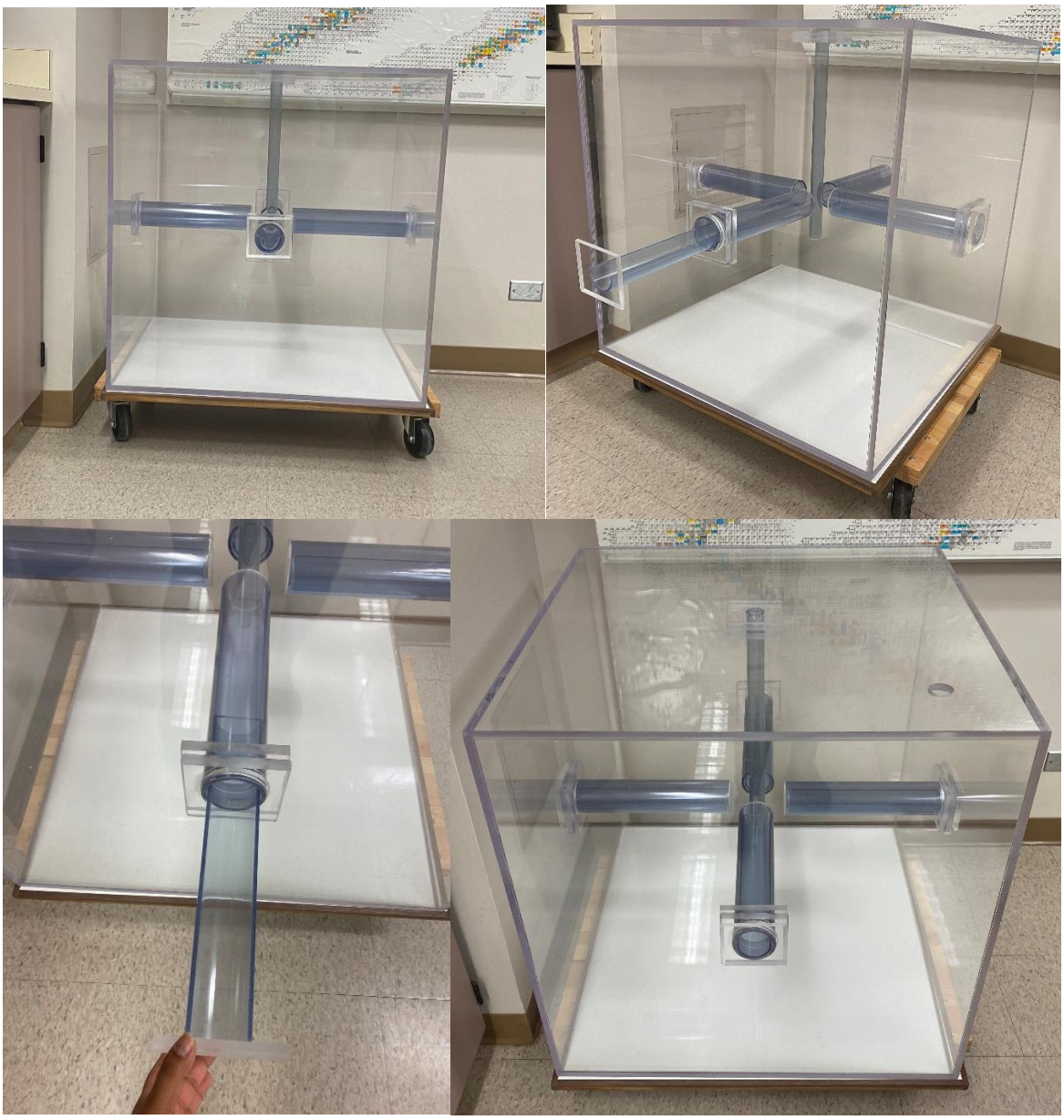

Figure 21: Completed tank (empty) in teaching lab.

5.2 Future Work

The completion of this initial phase of work opens the door to multiple additional projects regarding the Neutron Howitzer and water tank. Firstly, editing the MCNP model of the Neutron Howitzer should be done to determine if there are significant changes to the fluence results from minor changes in the geometry. Next, additional irradiations should be carried out in the

Howitzer to verify the effective curve in foils of other metals but also in irregularly shaped samples (test tubs and vials, rocks, coins, etc.). Finally, the techniques described in this thesis, MCNP modeling and NAA, will be repeated for the water tank, to determine the fluence intensities along the four sample drawers.

Bibliography

[1] Chadwick, J. (1932). "*The Existence of a Neutron. Proceedings of the Royal Society of London. Series A, Containing Papers of a Mathematical and Physical Character.*" 136(830), 692–708.

[2] Cember, H., & Johnson, T. E. (2009). "*Introduction to health physics (4th ed).*" McGraw-Hill Medical.

[3] Heilbronn, L. H. (n.d.). "*Neutron properties and definitions (supplement).*"

[4] Knoll, G. F. (2000). "*Radiation detection and measurement*" (3. ed). Wiley.

[5] INTERNATIONAL ATOMIC ENERGY AGENCY, "*Practical Aspects of Operating A Neutron Activation Analysis Laboratory."* IAEA-TECDOC-564, IAEA, Vienna (1990).

[6] De Soete, D., Gijbels, R., & Hoste, J. (1974). "*Neutron Activation Analysis (Vol. 34, Ser. Chemical Analysis: A Series of Monographs on Analytical Chemistry and its Applications).*" John Wiley & Sons Ltd.

[7] Holden, N E. "*Neutron capture cross section standards for BNL 325,*" Fourth Edition. United States. https://doi.org/10.2172/6280345

[8] Massimi, C., Domingo-Pardo, C., Vannini, G., Audouin, L., Guerrero, C., Abbondanno, U., Aerts, G., Alvarez, H., Alvarez-Velarde, F., Andriamonje, S., Andrzejewski, J., Assimakopoulos, P., Badurek, G., Baumann, P., Becvar, F., Belloni, F., Berthoumieux, E., Calvino, F., … Calviani, M. (2010). "*Au-197(n,gamma) cross section in the resonance region.*" *Physical Review. C, Nuclear Physics*, *81*(4). https://doi.org/10.1103/PhysRevC.81.044616

[9] Corvi, F., Stefanon, M., 1974. "*Gamma rays from resonance neutron capture in 115In."* Nucl. Phys. A 233, 185–216.

[10] Mughabghab, S. F. (n.d.). "*THERMAL NEUTRON CAPTURE CROSS SECTIONS RESONANCE INTEGRALS AND G-FACTORS.*" Brookhaven National Laboratory, International Nuclear Data Committee (INDC). TECDOC-564.

[11] Kopecky, J, Sublet, J C, Simpson, J A, Forrest, R A, & Nierop, D. "*Atlas of neutron capture cross sections.*" IAEA.

[12] "*Evaluated Nuclear Data File (ENDF).*" (n.d.). https://www.nndc.bnl.gov/endf/

[13] "*Model NH-3 Neutron Howitzer: Operation and Maintenance Manual.*" BK-066. Nuclear-Chicago Corporation, December (1959).

[14] "*The Design of Neutron Howitzers. International Journal of Applied Radiation and Isotopes.*" 1968, Vol 19. Pergamon Press, Northern Ireland.

[15] Pomerance, H.S. "*NUCLEAR ENGINEERING LABORATORY WITH A POINT NEUTRON SOURCE.*" report, March 17, 1958; Oak Ridge, Tennessee. (https://digital.library.unt.edu/ark:/67531/metadc1017666/: accessed February 13, 2024), University of North Texas Libraries, UNT Digital Library, https://digital.library.unt.edu; crediting UNT Libraries Government Documents Department.

[16] Guerra, F., Leone, M., & Robotti, N. (2006). "*Enrico Fermi's Discovery of Neutron-Induced Artificial Radioactivity: Neutrons and Neutron Sources. Physics in Perspective.*" 8(3), 255–281. https://doi.org/10.1007/s00016-006-0296-0

[17] Amendment for Radiation Project Application and Safety Plan for Room 002 Radiation Control Office Approval for Neutron Howitzer. Ref. # 22R-06-01. Colorado State University.

[18] Gilmore, G. (2008). "*Practical Gamma-Ray Spectrometry: Second Edition. Practical Gamma-Ray Spectrometry.*" 2nd Edition, by Gordon R. Gilmore. ISBN 978-0-470-86196-7. Published by Wiley-VCH Verlag, Weinheim,Germany, 2008. https://doi.org/10.1002/9780470861981

[19] Kulesza, J., Adams, T., Armstrong, J., Bolding, S., Brown, F., Bull, J., Burke, T., Clark, A., Forster Iii, R., Giron, J., Grieve, T., Josey, C., Martz, R., McKinney, G., Pearson, E., Rising, M., Solomon Jr., C., Swaminarayan, S., Trahan, T., … Zukaitis, A. (2022). "*MCNP® Code Version 6.3.0 Theory & User Manual*" (LA-UR-22-30006, 1889957; p. LA-UR-22-30006, 1889957). https://doi.org/10.2172/1889957

[20] Lee, D., Bucher, B. M., Krebs, K. M., Seabury, E. H., & Wharton, J. (2019). "*Determination of the Deuterium-Tritium (D-T) Generator Neutron Flux using Multi-foil Neutron Activation Analysis Method*" (INL/EXT-19-53812-Rev000, 1524045; p. INL/EXT-19-53812-Rev000, 1524045). https://doi.org/10.2172/1524045

[21] Mohamed Hammad E. "*Elemental Investigation of (Al-Cu) Alloys and Some Geological Samples using Neutron Activation and XRF Analysis Techniques.*" Minufiya University, Physics Master's Thesis (2012).

[22] Topuz, A. I., & Reyhancan, I. A. (2018). "*Neutronic Analysis of a Nuclear-Chicago NH3 Neutron Howitzer*" (arXiv:1806.05255). arXiv. http://arxiv.org/abs/1806.05255

[23] Topuz, A. I., & Reyhancan, I. A. (2018). "*3D Surface Radiation Dosimetry of a Nuclear-Chicago NH3 Neutron Howitzer*" (arXiv:1806.02387). arXiv. http://arxiv.org/abs/1806.02387

[24] Harvey Z. Neutron Flux and Energy Characterization of a Plutonium-Beryllium Isotopic "*Neutron Source by Mont- Carlo Simulation with Verification by Neutron Activation Analysis.*" University of Nevada Las Vegas, Health Physics Master's Thesis (2010).

[25] Detwiler, Rebecca S., McConn, Ronald J., Grimes, Thomas F., Upton, Scott A., & Engel, Eric J.. "*Compendium of Material Composition Data for Radiation Transport Modeling.*" United States. https://doi.org/10.2172/1782721

[26] Nguyen, C. T. "*Verification of the content, isotopic composition, and age of plutonium of Pu-Be neutron sources by gamma-spectroscopy.*" Institue of the Hungarian Academy of Sciences, 2005.

[27] Internationale Atomenergie-Organisation, & Internationale Atomenergie-Organisation (Eds.). (2001). *"Compendium of neutron spectra and detector responses for radiation protection purposes: Supplement to Technical reports series no. 318."* IAEA.

[28] AROUA, A., BOSCHUNG, M., CARTIER, F., GRECESCU, M., PRETRE, S., CERN "*Calibration Facility, Pu–Be source in different shieldings, Radiat. Prot. Dosim.*" 44 (1992)

[29] Vega-Carrillo, Héctor René et al. "Neutron and gamma-ray spectra of 239PuBe and 241AmBe." *Applied radiation and isotopes : including data, instrumentation*

and methods for use in agriculture, industry and medicine vol. 57,2 (2002): 167-70. doi:10.1016/s0969-8043(02)00083-0

[30] Hubbell, J.H., Photon Cross Sections, Attenuation Coefficients and Energy Absorption Coefficients from 10 keV to 100 GeV, Natl. Stand. Ref. Data Ser. **29** (1969).

[31] Newton B., "*Building an Acrylic Aquarium.*" Professional Plastics

APPENDIX I: MCNP Input Example

Text below is an example of the MCNP inputs used to simulate the neutron fluence in the neutron Howitzer drum. The code describes the irradiation of a gold foil at the 0 cm position in the sample channel.

```
Model NH-3 Howitzer Neutron Drum
c    Written by Anilu Diaz
c   Health Physics Master's Program Thesis
c    ***Full Fluence Spectrum, Au Foils***
c           *** 0cm position in sample channel ****
c     2023-2024
c
c
c _____CELLS CARD_____
c Void
9999 0     999  imp:n=0 $ void
c Air
999  3  -0.001205 -999 #20 #15 #10 #30 #40
          #35 #45 #60 #5 #25 #61 #62 #63 #64
          #50 #65 #75 #70 #66  imp:n=1
c DRUM
10   1  -2.6989   -100 110 #20 #30 #60 #35 #61 #62 #65
               #63 #64 #50 #75 #70 #66 imp:n=1
15   2  -0.812    -110 #20 #60 #30 #40
               #35 #45 #25 #61 #62 #63 #64 #65
               #50 #75 #70 #66 imp:n=1
5    1  -2.6989   -120 130 140 -150  imp:n=1 $ upper Al cyl
c SOURCE CHANNEL
20   1  -2.6989   -200 210        imp:n=1 $ source channel
30   3  -0.001205 -210 800 -220   imp:n=1 $ source channel Air inside
35   6  -1.19     -210 220        imp:n=1 $ fill sourch rod with plexiglass
25   3  -0.001205 -230            imp:n=1 $ source air pocket
c
40   5  -8       -800 810       imp:n=1 $ source cladding
45   4  -2.918  -810           imp:n=1 $source material
c SAMPLE CHANNEL
50   3  -0.001205  -500 904 -310 #70 #65 #66 #75 imp:n=1 $ sample channel air
60   6  -1.19      -700 400 -300 #50 #75 #65 #70 #66 imp:n=1 $ sample channel Al
c STORAGE PORTS
61   6  -1.19      -140 155 -165 #62 imp:n=1 $ storage port Al
62   3  -0.001205  -170              imp:n=1 $ storage port air
63   6  -1.19      -140 155 -160 #64 imp:n=1 $ storage port Al
64   3  -0.001205  -175              imp:n=1 $ storage port air
c Plastic Seperators & air pockets
65   7  -0.93     -310 903 -904     imp:n=1 $ seperator
```

```
66   3  -0.001205 -310 950 -903 #75 imp:n=1 $ air pocket
c
70   7  -0.93      -950 600 -310   imp:n=1 $ plastic plug
c Scandium Foils
75   8  -19.32 -900 901 -902       imp:n=1
c ***END OF CELLS***

c _____SURFACES CARD_____
c VOID
999  rcc 0 0 -55  0 0 120  45
c DRUM
100  rcc 0 0 -44.45  0 0 73.66  28.575   $ drum outer
110  rcc 0 0 -44.15  0 0 73.06  28.225   $ drum inner
120  c/z 0 0  28.575   $ outer drum cylinder
130  c/z 0 0  28.225   $ inner drum cylinder
140  pz  29.21         $ bottom of cylinder plane
150  pz  44.45         $ top of cylinder plane
c STORAGE PORTS (position assumed)
155  pz  11.33         $ bottom of source storage ports
165  c/z  1 7  1.666875 $ right source storage port, outer cylinder
170  rcc  1 7 11.43  0 0 17.78  1.566875 $ right source storage port air cylinder
160  c/z -7.5 2  1.666875 $ left source storage port, outer cylinder
175  rcc -7.5 2 11.43  0 0 17.78  1.566875 $ left source storage port air cylinder
c SOURCE CHANNEL
200  rcc 0 0 0    0 0 55.88  1.666875 $ outer source channel
210  rcc 0 0 0.3  0 0 55.28  1.566875 $ inner source channel
220  pz  4          $ plane concieling source space
230  rcc 0 0 -20.51  0 0 20.5  1.666875 $ air pocked for source unexposed
c SAMPLE CHANNEL
300  c/x  0 1.366875  2.79875  $ outer tube
310  c/x  0 1.366875  2.69875  $ inner tube
400  px 3.71    $ outer tube inner surface
500  px 30.38   $ inner tube outer surface
600  px 3.81    $ inner tube inner surface
700  px 30.48   $ outer tube outer surface
c
c
c 800  c/x 0 1.366875  11.43     $ drawer disk
c 810  px 30.78     $ drawer disk outer surface
c SOURCE
800  rcc 0 0 0.31  0 0 2.54    1.27 $ source cladding
810  rcc 0 0 0.36  0 0 2.44  1.17 $ source
c
c ***tally surfaces**
900  c/x 0 1.366875  0.6425  $ plastic plug/flux cylinder
950 px 5.08
```

```
c 4 foils, seperated by plastic spacer 4 cm thick
901  px  5.081
902  px  5.161
c
903  px  5.162
904  px  17.162
c ***END OF SURFACES***

c _____MATERIALS CARD_____
c Pure Al, 2.6989 g/cm^3  #6
m1   13027 -1.0
c mt1  al27.20t
c
c Paraffin, #396  0.812 g/cm^3
m2   1001 -0.148579
     1002 -0.000034
     6000 -0.851387
mt2  lwtr.20t
c
c Dry Air, 0.001205 g/cm^3
m3   6012  -0.000125
     7014  -0.75525
     8016  -0.2318
     18000 -0.01282
c
c Plutonium/Beryllium Source p = 2.918 g/cm^3
m4   94237  -1E-10      $ Pu-237
     94238  -5.451E-4   $ Pu-238
     94239  -5.486E-2   $ Pu-239
     94240  -1.013E-2   $ Pu-240
     94241  -4.946E-2   $ Pu-241
     94242  -8.787E-4   $ Pu-242
     04009  -8.8413E-1  $ Be-9
c
c Stainless Steel 316 #333, 8 g/cm^3
m5   06000 -0.000800 $ C
     25055 -0.020000 $ Mn-55
     15031 -0.000450 $ P-31
     16000 -0.000300 $ S
     14000 -0.010000 $ Si
     24000 -0.170000 $ Cr
     28000 -0.120000 $ Ni
     42000 -0.025000 $ Mn
     26000 -0.653450 $ Fe
c
c C5H8O2, Plexygrass, NIST 1.19 g/cm^3
```

```
m6   1001 -0.080522
     1002 -0.000019
     6000 -0.599846
     8016 -0.318747
     8017 -0.000866
c
c Plastic, Polyethylene non-borated #275, 0.93 g/cm^3
m7   1001 -0.143686 $ H-1
     1002 -0.000033 $ H-2
     6000 -0.856281 $ C
mt7  poly.20t
c Pure Au, 19.32 g/cm^3
m8   79197 -1.0
c ____________________SOURCE/TALLIES CARD_____________________________
nps 1e7
mode n
c
sdef axs=0 0 1 pos= 0 0 0.36 rad=d1 ext=d2 erg=d3 par=1
si1   0 1.17
sp1  -21 1
si2   0 2.44
sp2  0 1
si3  1.00E-09 2.20E-09 4.60E-09 1.00E-08 2.20E-08 4.60E-08 1.00E-07 2.10E-07
     4.60E-07 1.00E-06 2.20E-06 4.60E-06 1.00E-05 2.20E-05 4.60E-05 1.00E-04
     2.20E-04 4.60E-04 1.00E-03 2.20E-03 4.60E-03 1.00E-02 1.30E-02 1.60E-02
     2.00E-02 2.50E-02 3.20E-02 4.00E-02 5.00E-02 6.30E-02 7.90E-02 1.00E-01
     1.30E-01 1.60E-01 2.00E-01 2.50E-01 3.20E-01 4.00E-01 5.00E-01 6.30E-01
     7.90E-01 1.00E+00 1.30E+00 1.60E+00 2.00E+00 2.50E+00 3.20E+00 4.00E+00
     5.00E+00 6.30E+00 7.90E+00 1.00E+01 1.60E+01 2.50E+01 4.00E+01 6.30E+01
     1.00E+02 1.60E+02 2.50E+02 4.00E+02 6.30E+02
sp3  0.00E+00 1.81E-02 1.81E-02 1.81E-02 1.70E-02 1.60E-02 1.40E-02 8.32E-03
     4.51E-03 1.40E-02 3.51E-03 2.61E-03 1.20E-02 7.12E-03 5.01E-03 4.51E-03
     7.02E-03 1.60E-02 8.22E-03 7.42E-03 9.13E-03 7.92E-03 6.12E-03 5.01E-03
     1.20E-03 5.72E-03 3.91E-03 1.91E-02 1.60E-02 1.10E-02 1.10E-02 1.81E-02
     3.21E-02 7.42E-02 7.62E-02 5.62E-02 6.72E-02 7.62E-02 8.93E-02 5.42E-02
     1.91E-01 2.81E-01 2.21E-01 1.81E-01 2.41E-02 1.50E-01 6.22E-01 4.81E-01
     4.31E-01 2.81E-01 1.30E-01 7.82E-03 4.11E-04 0.00E+00 0.00E+00 0.00E+00
     0.00E+00 0.00E+00 0.00E+00 0.00E+00 0.00E+00
c
c
c *******Tallies,Foil only*********
f104:n 75
e104 0 2.5e-8 5e-7 3e-6 1e-5 1e-3 5e-3 1e-2 1e-1 1 3 5 7 10 13 15
print
```

APPENDIX II: MCNP Output Results

Table 11: MCNP simulated energy fluence results for air filled sample channel. The position for each fluence listed is in reference to the inner end of the sample channel.

		Tally Fluence Energy Ranges					
Tally	Position (cm)	Thermal	Resonance (3 eV)	Resonance (5 keV)	Slow	Fast	Total
104	0	8.72E+03	3.00E+04	3.79E+04	4.18E+04	1.73E+04	6.78E+04
114	2	7.40E+03	2.46E+04	3.00E+04	3.26E+04	1.08E+04	5.08E+04
124	4	6.04E+03	1.95E+04	2.33E+04	2.52E+04	7.46E+03	3.87E+04
134	6	4.80E+03	1.53E+04	1.80E+04	1.94E+04	5.46E+03	2.96E+04
144	8	3.80E+03	1.19E+04	1.39E+04	1.48E+04	4.14E+03	2.28E+04
154	10	2.96E+03	9.20E+03	1.07E+04	1.14E+04	3.23E+03	1.76E+04
164	12	2.31E+03	7.08E+03	8.20E+03	8.75E+03	2.56E+03	1.36E+04
174	14	1.77E+03	5.44E+03	6.28E+03	6.70E+03	2.06E+03	1.05E+04
184	16	1.35E+03	4.10E+03	4.74E+03	5.08E+03	1.68E+03	8.11E+03
194	18	9.93E+02	3.02E+03	3.51E+03	3.77E+03	1.39E+03	6.15E+03
204	20	6.92E+02	2.10E+03	2.47E+03	2.68E+03	1.16E+03	4.53E+03
214	22	4.12E+02	1.29E+03	1.55E+03	1.71E+03	9.62E+02	3.08E+03
224	24	2.69E+02	8.57E+02	1.06E+03	1.18E+03	8.18E+02	2.27E+03
		Uncertainties					
Tally	Position (cm)	Thermal	Resonance (3 eV)	Resonance (5 keV)	Slow	Fast	Total
104	0	2.27E+01	4.92E+01	5.40E+01	5.60E+01	2.87E+01	7.46E+01
114	2	2.00E+01	4.05E+01	4.45E+01	4.61E+01	2.23E+01	6.10E+01
124	4	1.75E+01	3.43E+01	3.74E+01	3.87E+01	1.85E+01	5.42E+01
134	6	1.54E+01	2.99E+01	3.25E+01	3.61E+01	1.60E+01	4.45E+01
144	8	1.33E+01	2.67E+01	2.87E+01	2.97E+01	1.37E+01	3.87E+01
154	10	1.16E+01	2.25E+01	2.43E+01	2.51E+01	1.22E+01	3.34E+01
164	12	1.02E+01	2.01E+01	2.16E+01	2.23E+01	1.08E+01	3.00E+01
174	14	8.86E+00	1.71E+01	1.84E+01	1.90E+01	9.68E+00	2.53E+01
184	16	7.70E+00	1.49E+01	1.61E+01	1.66E+01	8.72E+00	2.19E+01

194	18	6.56E+00	1.25E+01	1.35E+01	1.40E+01	7.91E+00	1.91E+01
204	20	5.33E+00	9.93E+00	1.09E+01	1.13E+01	7.19E+00	1.54E+01
214	22	3.75E+00	6.85E+00	7.76E+00	8.23E+00	6.49E+00	1.14E+01
224	24	3.06E+00	5.49E+00	6.35E+00	6.80E+00	6.01E+00	9.75E+00

Table 12: MCNP simulated energy fluence results for air filled sample channel. The position for each fluence listed is in reference to the inner end of the sample channel.

		Tally Fluence Energy Ranges					
Tally	Position (cm)	Thermal	Resonance (3 eV)	Resonance (5 keV)	Slow	Fast	Total
104	0	1.33E+04	4.53E+04	5.43E+04	5.84E+04	1.62E+04	8.79E+04
114	2	8.87E+03	2.94E+04	3.37E+04	3.56E+04	7.36E+03	5.18E+04
124	4	5.55E+03	1.80E+04	2.01E+04	2.10E+04	3.66E+03	3.02E+04
134	6	3.42E+03	1.10E+04	1.21E+04	1.25E+04	1.96E+03	1.79E+04
144	8	2.09E+03	6.62E+03	7.22E+03	7.48E+03	1.10E+03	1.07E+04
154	10	1.26E+03	4.00E+03	4.34E+03	4.49E+03	6.49E+02	6.40E+03
164	12	7.70E+02	2.43E+03	2.63E+03	2.72E+03	3.89E+02	3.88E+03
174	14	4.76E+02	1.49E+03	1.61E+03	1.67E+03	2.36E+02	2.38E+03
184	16	2.89E+02	9.13E+02	9.90E+02	1.02E+03	1.49E+02	1.46E+03
194	18	1.73E+02	5.38E+02	5.82E+02	6.02E+02	9.53E+01	8.70E+02
204	20	9.16E+01	2.91E+02	3.19E+02	3.31E+02	6.12E+01	4.84E+02
214	22	3.42E+01	1.10E+02	1.25E+02	1.32E+02	3.76E+01	2.03E+02
224	24	9.36E+00	3.41E+01	4.13E+01	4.43E+01	2.59E+01	7.96E+01
		Uncertainties					
Tally	Position (cm)	Thermal	Resonance (3 eV)	Resonance (5 keV)	Slow	Fast	Total
104	0	2.67E+01	7.36E+01	7.59E+01	7.68E+01	2.68E+01	1.14E+02
114	2	2.13E+01	5.96E+01	6.10E+01	6.15E+01	1.84E+01	8.80E+01
124	4	1.66E+01	4.55E+01	4.64E+01	4.67E+01	1.29E+01	6.65E+01
134	6	1.30E+01	3.53E+01	3.59E+01	3.61E+01	9.54E+00	5.19E+01
144	8	1.00E+01	2.65E+01	2.70E+01	2.71E+01	7.16E+00	3.95E+01

154	10	7.58E+00	2.07E+01	2.11E+01	2.12E+01	5.59E+00	3.01E+01
164	12	5.93E+00	1.60E+01	1.62E+01	1.63E+01	4.30E+00	2.33E+01
174	14	4.66E+00	1.25E+01	1.26E+01	1.27E+01	3.37E+00	1.83E+01
184	16	3.64E+00	9.76E+00	9.92E+00	9.99E+00	2.67E+00	1.43E+01
194	18	2.82E+00	7.45E+00	7.57E+00	7.61E+00	2.16E+00	1.10E+01
204	20	2.06E+00	5.53E+00	5.63E+00	5.66E+00	1.72E+00	8.13E+00
214	22	1.22E+00	3.20E+00	3.30E+00	3.33E+00	1.36E+00	4.90E+00
224	24	6.71E-01	1.69E+00	1.81E+00	1.84E+00	1.18E+00	2.79E+00

Table 13: MCNP simulated energy fluence results for gold foils in sample channel.

Energy (MeV)	0 cm Foil				4 cm Foil				8 cm Foil			
	Tally	Error	Fluence	Uncertainty	Tally	Error	Fluence	Uncertainty	Tally	Error	Fluence	Uncertainty
0.00E+00	0.00E+00	0.00E+00	0.00E+00	0.00E+00	0.00E+00	0.00E+00	0.00E+00	0.00E+00	0.00E+00	0.00E+00	0.00E+00	0.00E+00
2.50E-08	6.66E-04	1.13E-02	6.66E+03	7.52E+01	3.65E-04	1.36E-02	3.65E+03	4.97E+01	8.95E-05	2.81E-02	8.95E+02	2.51E+01
5.00E-07	6.66E-04	1.13E-02	6.66E+03	7.52E+01	1.54E-03	8.00E-03	1.54E+04	1.23E+02	4.53E-04	1.56E-02	4.53E+03	7.07E+01
3.00E-06	2.65E-04	2.54E-02	2.65E+03	6.72E+01	6.59E-05	5.09E-02	6.59E+02	3.36E+01	1.83E-05	8.81E-02	1.83E+02	1.61E+01
1.00E-05	1.25E-04	3.49E-02	1.25E+03	4.35E+01	2.86E-05	6.89E-02	2.86E+02	1.97E+01	6.03E-06	1.23E-01	6.03E+01	7.40E+00
1.00E-03	8.36E-04	1.64E-02	8.36E+03	1.37E+02	1.85E-04	3.34E-02	1.85E+03	6.18E+01	4.42E-05	7.03E-02	4.42E+02	3.11E+01
5.00E-03	3.11E-04	2.61E-02	3.11E+03	8.11E+01	6.12E-05	5.89E-02	6.12E+02	3.61E+01	1.63E-05	1.03E-01	1.63E+02	1.68E+01
1.00E-02	1.45E-04	3.84E-02	1.45E+03	5.57E+01	3.14E-05	8.09E-02	3.14E+02	2.54E+01	5.49E-06	1.59E-01	5.49E+01	8.73E+00
1.00E-01	5.47E-04	1.95E-02	5.47E+03	1.07E+02	1.06E-04	4.74E-02	1.06E+03	5.05E+01	3.01E-05	9.16E-02	3.01E+02	2.76E+01
1.00E+00	1.12E-03	1.17E-02	1.12E+04	1.31E+02	2.09E-04	2.82E-02	2.09E+03	5.90E+01	5.38E-05	5.43E-02	5.38E+02	2.92E+01
3.00E+00	9.65E-04	1.12E-02	9.65E+03	1.08E+02	1.98E-04	2.52E-02	1.98E+03	5.00E+01	5.38E-05	4.66E-02	5.38E+02	2.51E+01
5.00E+00	5.28E-04	1.28E-02	5.28E+03	6.76E+01	9.44E-05	3.21E-02	9.44E+02	3.03E+01	2.65E-05	5.93E-02	2.65E+02	1.57E+01
7.00E+00	1.67E-04	2.21E-02	1.67E+03	3.69E+01	3.25E-05	4.96E-02	3.25E+02	1.61E+01	1.16E-05	8.75E-02	1.16E+02	1.01E+01
1.00E+01	3.87E-05	4.41E-02	3.87E+02	1.71E+01	8.09E-06	9.71E-02	8.09E+01	7.86E+00	2.47E-06	1.74E-01	2.47E+01	4.29E+00
1.30E+01	5.95E-07	3.15E-01	5.95E+00	1.87E+00	9.17E-08	7.76E-01	9.17E-01	7.11E-01	1.07E-07	7.28E-01	1.07E+00	7.78E-01
1.50E+01	1.25E-07	7.26E-01	1.25E+00	9.07E-01	1.36E-07	7.13E-01	1.36E+00	9.72E-01	0.00E+00	0.00E+00	0.00E+00	0.00E+00
total	9.05E-03	4.20E-03	9.05E+04	3.80E+02	2.92E-03	6.60E-03	2.92E+04	1.93E+02	8.11E-04	1.27E-02	8.11E+03	1.03E+02

Table 14: MCNP tally results for gold foils categorized into energy ranges and their uncertainties.

Position (cm)	Thermal	Resonance (5 keV)	Slow	Fast	Total
0.00E+00	6.66E+03	2.20E+04	3.56E+04	2.82E+04	9.05E+04
4.00E+00	3.65E+03	1.88E+04	2.38E+04	5.43E+03	2.92E+04
8.00E+00	8.95E+02	5.38E+03	6.63E+03	1.48E+03	8.11E+03
Uncertainties					
Position (cm)	Thermal	Resonance (5 keV)	Slow	Fast	Total
0.00E+00	7.52E+01	1.93E+02	2.40E+02	1.87E+02	3.80E+02
4.00E+00	4.97E+01	1.48E+02	1.66E+02	8.50E+01	1.93E+02
8.00E+00	2.51E+01	8.10E+01	8.96E+01	4.30E+01	1.03E+02

Table 15: MCNP simulated energy fluence results for indium foils in sample channel.

Energy (MeV)	0 cm Foil				4 cm Foil				8 cm Foil			
	Tally	Error	Fluence	Uncertainty	Tally	Error	Fluence	Uncertainty	Tally	Error	Fluence	Uncertainty
0.00E+00	0.00E+00	0.00E+00	0.00E+00	0.00E+00	0.00E+00	0.00E+00	0.00E+00	0.00E+00	0.00E+00	0.00E+00	0.00E+00	0.00E+00
2.50E-08	5.61E-04	1.16E-02	5.61E+03	6.51E+01	2.81E-04	1.49E-02	2.81E+03	4.19E+01	7.61E-05	2.83E-02	7.61E+02	2.15E+01
5.00E-07	2.91E-03	6.30E-03	2.91E+04	1.83E+02	1.22E-03	8.60E-03	1.22E+04	1.05E+02	3.75E-04	1.62E-02	3.75E+03	6.08E+01
3.00E-06	1.64E-04	2.87E-02	1.64E+03	4.70E+01	4.49E-05	5.51E-02	4.49E+02	2.47E+01	1.26E-05	9.56E-02	1.26E+02	1.21E+01
1.00E-05	1.89E-04	3.11E-02	1.89E+03	5.88E+01	4.50E-05	6.44E-02	4.50E+02	2.90E+01	1.05E-05	1.13E-01	1.05E+02	1.19E+01
1.00E-03	8.39E-04	1.65E-02	8.39E+03	1.38E+02	1.90E-04	3.39E-02	1.90E+03	6.44E+01	4.45E-05	6.84E-02	4.45E+02	3.04E+01
5.00E-03	3.10E-04	2.59E-02	3.10E+03	8.02E+01	5.97E-05	5.67E-02	5.97E+02	3.39E+01	1.65E-05	1.11E-01	1.65E+02	1.82E+01
1.00E-02	1.45E-04	3.88E-02	1.45E+03	5.62E+01	2.83E-05	8.21E-02	2.83E+02	2.33E+01	5.25E-06	1.55E-01	5.25E+01	8.15E+00
1.00E-01	5.36E-04	1.94E-02	5.36E+03	1.04E+02	1.03E-04	4.59E-02	1.03E+03	4.73E+01	3.01E-05	9.13E-02	3.01E+02	2.75E+01
1.00E+00	1.11E-03	1.18E-02	1.11E+04	1.31E+02	2.11E-04	2.85E-02	2.11E+03	6.01E+01	5.36E-05	5.72E-02	5.36E+02	3.06E+01
3.00E+00	9.57E-04	1.11E-02	9.57E+03	1.06E+02	1.97E-04	2.42E-02	1.97E+03	4.77E+01	5.37E-05	4.58E-02	5.37E+02	2.46E+01
5.00E+00	5.30E-04	1.29E-02	5.30E+03	6.84E+01	9.32E-05	3.14E-02	9.32E+02	2.93E+01	2.66E-05	6.11E-02	2.66E+02	1.62E+01
7.00E+00	1.68E-04	2.21E-02	1.68E+03	3.71E+01	3.22E-05	4.99E-02	3.22E+02	1.61E+01	1.14E-05	8.71E-02	1.14E+02	9.95E+00
1.00E+01	3.88E-05	4.41E-02	3.88E+02	1.71E+01	8.40E-06	9.54E-02	8.40E+01	8.02E+00	2.55E-06	1.69E-01	2.55E+01	4.31E+00
1.30E+01	5.95E-07	3.15E-01	5.95E+00	1.87E+00	1.28E-07	6.26E-01	1.28E+00	8.00E-01	1.04E-07	7.34E-01	1.04E+00	7.65E-01
1.50E+01	1.25E-07	7.26E-01	1.25E+00	9.07E-01	7.71E-08	1.00E+00	7.71E-01	7.71E-01	0.00E+00	0.00E+00	0.00E+00	0.00E+00
total	8.46E-03	4.20E-03	8.46E+04	3.55E+02	2.51E-03	7.10E-03	2.51E+04	1.78E+02	7.19E-04	1.33E-02	7.19E+03	9.56E+01

Table 16: MCNP tally results for indium foils categorized into energy ranges and their uncertainties.

Position (cm)	Thermal	Resonance (5 keV)	Slow	Fast	Total
0.00E+00	5.61E+03	3.08E+04	5.65E+04	2.81E+04	8.46E+04
4.00E+00	2.81E+03	1.26E+04	1.97E+04	5.42E+03	2.51E+04
8.00E+00	7.61E+02	3.88E+03	5.71E+03	1.48E+03	7.19E+03
Uncertainties					
Position (cm)	Thermal	Resonance (5 keV)	Slow	Fast	Total
0.00E+00	6.51E+01	1.89E+02	2.88E+02	1.87E+02	3.55E+02
4.00E+00	4.19E+01	1.08E+02	1.49E+02	8.41E+01	1.78E+02
8.00E+00	2.15E+01	6.20E+01	8.08E+01	4.39E+01	9.56E+01

APPENDIX III: NAA Details

Table 17: Gold foil NAA photopeaks measured and times recorded.

Position:	0 cm			
Foil: A	Channel:	Left	Foil Mass (g):	0.1192
	Detector:	Joliot	Target Atoms:	3.6444E+20
Peak Energy (keV)	Area (counts)	Uncertainty	Efficiency %	Efficiency % Uncertainty
412.24	1.69E+06	1.31E+03	8.70E+00	1.54E+00
	Times (s)			
Irradiation	3.456E+05 ± 60			
Count (Live)	2.16E+04 ± 0			
Transfer	2.17E+02 ± 3			
Foil: D+Cd	Channel:	Left	Foil Mass (g):	0.1219
	Detector:	Curie	Target Atoms:	3.7269E+20
Peak Energy (keV)	Area (counts)	Uncertainty	Efficiency %	Efficiency % Uncertainty
410.18	1.26E+04	3.84E+02	2.61E-01	4.91E-03
	Times (s)			
Irradiation	3.456 E+05 ± 60			
Count (Live)	2.16E+04 ± 0			
Transfer	2.41E+02 ± 3			

Position:	4 cm			
Foil: B	Channel:	Right	Foil Mass (g):	0.1201
	Detector:	Joliot	Target Atoms:	3.672E+20
Peak Energy (keV)	Area (counts)	Uncertainty	Efficiency %	Efficiency % Uncertainty
412.24	1.13E+06	1.08E+03	8.70E+00	1.54E+00
	Times (s)			
Irradiation	3.456E+05 ± 60			
Count (Live)	2.16E+04 ± 0			
Transfer	2.74E+02 ± 3			
Foil: B+Cd	Channel:	Right	Foil Mass (g):	0.1201
	Detector:	Joliot	Target Atoms:	3.672E+20
Peak Energy (keV)	Area (counts)	Uncertainty	Efficiency %	Efficiency % Uncertainty
410.18	1.07E+05	3.30E+03	8.71E+00	1.54E+00
	Times (s)			
Irradiation	3.456E+05 ± 60			
Count (Live)	2.16E+04 ± 0			
Transfer	2.2E+02 ± 3			

Position:	8 cm			
Foil: C	Channel:	Left	Foil Mass (g):	0.1219
	Detector:	Curie	Target Atoms:	3.7269E+20
Peak Energy (keV)	Area (counts)	Uncertainty	Efficiency %	Efficiency % Uncertainty
410.18	3.45E+04	6.31E+02	2.61E-01	4.92E-03
	Times (s)			
Irradiation	3.456E+05 ± 60			
Count (Live)	2.16E+04 ± 0			
Transfer	2.4E+03 ± 3			
Foil: C+Cd	Channel:	Left	Foil Mass (g):	0.1209
	Detector:	Joliot	Target Atoms:	3.6963E+20
Peak Energy (keV)	Area (counts)	Uncertainty	Efficiency %	Efficiency % Uncertainty
412.24	3.66E+04	2.10E+02	8.71E+00	1.54E+00
	Times (s)			
Irradiation	3.5328E+05 ± 60			
Count (Live)	2.16E+04 ± 0			
Transfer	2.6E+02 ± 3			

Table 18: Indium foil NAA photopeaks measured and times recorded.

Position:	0 cm			
Foil: V	Channel:	Left	Foil Mass (g):	0.1184
	Detector:	Joliot	Target Atoms:	5.935E+20
Peak Energy (keV)	Area (counts)	Uncertainty	Efficiency %	Efficiency % Uncertainty
336.29	2.86E+03	2.67E+02	9.41E+00	1.49E+00
416.94	2.38E+05	5.67E+02	8.66E+00	1.55E+00
818.68	5.19E+04	3.92E+02	4.44E+00	4.97E-01
1097.21	2.44E+05	5.00E+02	3.06E+00	2.89E-01
1293.42	2.99E+05	5.79E+02	2.54E+00	1.60E-01
2112.04	3.75E+04	2.24E+02	2.12E+00	2.80E+00
	Times (s)			
Irradiation	2.16E+04 ± 60			
Count (Live)	4.32E+04 ± 0			
Transfer	1.87E+02± 3			
Foil: Y+Cd	Channel:	Left	Foil Mass (g):	0.1196
	Detector:	Joliot	Target Atoms:	5.9952E+20
Peak Energy (keV)	Area (counts)	Uncertainty	Efficiency %	Efficiency % Uncertainty
336.29	336.29	3.29E+03	9.41E+00	1.49E+00
416.94	416.99	2.76E+04	8.66E+00	1.55E+00
818.68	818.75	6.10E+03	4.44E+00	4.97E-01
1097.21	1097.32	2.89E+04	3.06E+00	2.89E-01
1293.42	1293.55	3.46E+04	2.54E+00	1.60E-01
2112.04	2112.2	4.38E+03	2.12E+00	2.80E+00
	Times (s)			
Irradiation	2.16E+04 ± 60			
Count (Live)	4.32E+04 ± 0			
Transfer	2.36E+02± 3			

Position:	4 cm			
Foil: W	Channel:	Left	Foil Mass (g):	0.1214
	Detector:	Joliot	Target Atoms:	6.0854E+20
Peak Energy (keV)	Area (counts)	Uncertainty	Efficiency %	Efficiency % Uncertainty
336.29	5.56E+02	2.29E+02	9.41E+00	1.49E+00
416.94	1.85E+05	4.23E+02	8.66E+00	1.55E+00
818.68	3.93E+04	3.41E+02	4.44E+00	4.97E-01
1097.21	1.89E+05	440.42	3.06E+00	2.89E-01
1293.42	2.30E+05	509.62	2.54E+00	1.60E-01
2112.04	2.93E+04	201.55	2.12E+00	2.80E+00
	Times (s)			
Irradiation	2.16E+04 ± 60			
Count (Live)	4.32E+04 ± 0			
Transfer	2.08E+02± 3			
Foil: X+Cd	Channel:	Left	Foil Mass (g):	0.1254
	Detector:	Joliot	Target Atoms:	6.2859E+20
Peak Energy (keV)	Area (counts)	Uncertainty	Efficiency %	Efficiency % Uncertainty
336.29	9.09E+02	1.49E+02	9.41E+00	1.49E-+00
416.94	1.35E+04	1.74E+02	8.66E+00	1.55E+00
818.68	2.85E+03	1.14E+02	4.44E+00	4.97E-01
1097.21	1.37E+04	1.48E+02	3.06E+00	2.89E-01
1293.42	1.66E+04	1.46E+02	2.54E+00	1.60E-02
2112.04	2.01E+03	6.31E+01	2.12E+00	2.80E+00
	Times (s)			
Irradiation	2.16E+04 ± 60			
Count (Live)	4.32E+04 ± 0			
Transfer	1.87E+02± 3			

Position:	8 cm			
Foil: X	Channel:	Right	Foil Mass (g):	0.1254
	Detector:	Joliot	Target Atoms:	6.28593E+20
Peak Energy (keV)	Area (counts)	Uncertainty	Efficiency %	Efficiency % Uncertainty
336.29	2.53E+03	1.33E+02	9.41E+00	1.49E+00
416.94	2.74E+04	2.02E+02	8.65E+00	1.55E+00
818.68	5.85E+03	1.45E+02	4.44E+00	4.97E-01
1097.21	2.87E+04	1.75E+02	3.06E+00	2.89E-01
1293.42	3.45E+04	2.02E+02	2.54E+00	1.60E-01
2112.04	4.34E+03	8.05E+01	2.12E+00	2.80E+00
	Times (s)			
Irradiation	2.16E+04 ± 60			
Count (Live)	2.16E+04 ± 0			
Transfer	3.06E+02± 3			
Foil: X+Cd	Channel:	Right	Foil Mass (g):	0.1254
	Detector:	Curie	Target Atoms:	6.28593E+20
Peak Energy (keV)	Area (counts)	Uncertainty	Efficiency %	Efficiency % Uncertainty
336.29	0.00E+00	0.00E+00	0.00E+00	0.00E+00
416.94	1.76E+03	8.73E+01	7.98E-01	1.50E-02
818.68	0.00E+00	0.00E+00	0.00E+00	0.00E+00
1097.21	1.00E+03	7.89E+01	2.77E-01	2.86E-03
1293.42	8.57E+02	8.59E+01	2.42E-01	1.61E-03
2112.04	0.00E+00	0.00E+00	0.00E+00	0.00E+00
	Times (s)			
Irradiation	2.16E+04 ± 60			
Count (Live)	2.16E+04 ± 0			
Transfer	2.81E+02± 3			

ANILU S. DIAZ RUIZ

1614 FOXBROOK WY
FORT COLLINS CO, 80526
(843)-409-6738
DIAZANILUSOFIA@GMAIL.COM
ANILU.DIAZ@COLOSTATE.EDU
WWW.LINKEDIN.COM/IN/ANILUDIAZ

EDUCATION

Bachelor of Science | Francis Marion University
AUGUST 2017–APRIL 2022
Major: Health Physics
Minor: Mathematics and Chemistry

Master of Science in Radiological Health | Colorado State University
AUGEST 2022–CURRENT
Program: Health Physics Specialization
Department: Environmental & Radiological Health Sciences

EXPERIENCE

Lab Assistant| Francis Marion University Physics Department
AUGEST 2021 – DECEMBER 2021
JANUARY 2021 – APRIL 2021
- Enhanced students' understanding of physics and chemistry
- Assisted in developing students' laboratory report writing skills
- Facilitated student's correct utilization of lab equipment

Health Physics Summer Intern| Savannah River Nuclear Solutions
JUNE 2021 – AUGUST 2021
- Trained in the use of gamma irradiators
- Experienced writing exposure meter evaluation reports
- Trained in the use and handling of radioactive materials

Research Assistant | Professor Led Yeast Biosensor Research
JANUARY 2021 – APRIL 2021
- Assisted professor in dissertation work
- Sorted and analyzed data gathered from liquid scintillation of multiple samples

Graduate Summer Intern| Los Alamos National Laboratory
JUNE 2023 – AUGUST 2023
- Completed MCNP Safeguards Training
- Reported on MCNP Spent Fuel Transport Modeling for XCP-7 Group
- Received training in MCNP programing and Performing Tasks in High Performance Computers

ACOMPLISHMENTS

- Awarded the Savannah River Chapter –Health Physics Society Roscoe Hall Memorial
- Awarded the Francis Marion University Health Physics Award from the 2022 Academic Awards Program.

PRESENTATIONS

- 2023 Spring, Central Rocky Mountain Chapter Health Physics Society Colorado State University Technical Meeting, “Flux Calculations of PuBe source and Neutron Howitzer Drum”
- 2024 Spring, CVMBS Research Showcase, “Neutron Flux in a Howitzer Drum”
- 2024 Spring, Hirosaki University Delegation Health Physics Research Presentations, “Neutron Fluence in a Howitzer Drum and MCNP Modeling”
- 2024 Spring, Central Rocky Mountain Chapter Health Physics Society Colorado State University Technical Meeting, “Neutron Fluence in a Howitzer Drum and Construction of a Water-Moderated Neutron Irradiator”